Physics of Fluids

RESEARCH ARTICLE | DECEMBER 24 2025

On what can or cannot influence the small amplitude oscillations of a gas bubble

F. Brini ; L. Seccia

Check for updates

Physics of Fluids 37, 127145 (2025)
https://doi.org/10.1063/5.0305369

View Online
Export Citation

Articles You May Be Interested In

The role of the dynamic pressure in the behavior of an oscillating gas bubble

Physics of Fluids (September 2024)

Scattering from a pair of closely spaced bubbles

J. Acoust. Soc. Am. (July 2018)

A model for acoustic vaporization of encapsulated droplets

J. Acoust. Soc. Am. (December 2015)

10 January 2026 08:22:20

AIP Publishing

AIP Publishing
Physics of Fluids
Special Topics Open for Submissions
Learn More

Physics of Fluids ARTICLE pubs.aip.org/aip/pof

On what can or cannot influence the small amplitude oscillations of a gas bubble

Cite as: Phys. Fluids **37**, 127145 (2025); doi: 10.1063/5.0305369
Submitted: 6 October 2025 · Accepted: 28 November 2025 ·
Published Online: 24 December 2025

View Online Export Citation CrossMark

F. Brini[a] and L. Seccia[b]

AFFILIATIONS

Department of Mathematics, University of Bologna via Saragozza, 8 I-40123 Bologna, Italy

[a]Author to whom the correspondence should be addressed: francesca.brini@unibo.it
[b]Electronic mail: leonardo.seccia@unibo.it

ABSTRACT

The analysis presented in this paper concerns the impact of different physical quantities and conditions on the small amplitude oscillations of a single gas bubble immersed in a liquid, in the presence of an acoustic forcing pressure. Namely, effects related to the nature of the gas and its modeling, to the boundary conditions on the bubble wall, and to the size and shape of the bubble itself are studied and compared. The solutions are always determined analytically. The polytropic index and the damping coefficient are not assigned *a priori* but are determined from gas dynamics equations of Navier–Stokes–Fourier, and rational extended thermodynamics type. This preliminary approach facilitates the distinction between essential features and reasonable possible simplifications, also with a view to extending the model to nonlinear regimes. Furthermore, the results obtained could suggest how to prescribe the polytropic index more accurately when the gas dynamics in the bubble are reduced to a simple polytropic process.

© *2025 Author(s). All article content, except where otherwise noted, is licensed under a Creative Commons Attribution-NonCommercial-NoDerivs 4.0 International (CC BY-NC-ND) license (https://creativecommons.org/licenses/by-nc-nd/4.0/).* https://doi.org/10.1063/5.0305369

10 January 2026 08:22:20

I. INTRODUCTION

The dynamics of gas bubbles immersed in a liquid is a fascinating and current research topic and a framework for new discoveries, even more than a century after Lord Rayleigh's pioneering studies.[1] This is demonstrated by the huge literature on the subject (Refs. 2–16 are just a tiny fraction of the available references) as well as by the new applications that are constantly being introduced in medicine, science, and engineering to overcome problems previously considered intractable. For example, one might refer to treatment of degenerative brain diseases,[17–19] water purification,[20] and sonochemistry.[21,22] These applied results are complemented by theoretical studies aimed at achieving a deeper understanding of the complex phenomena associated with bubbles, in order to better control and predict their behavior.

Despite the introduction of increasingly sophisticated models, much remains to be investigated. It should also be remarked that the small size of bubbles often prevents detailed experimental observation of what occurs within them. In the field of bubble dynamics, one of the most studied problems is that associated with the presence of an acoustic force that generates oscillations in the liquid and, consequently, periodic behaviors in the bubbles immersed in that liquid.

There are two main reasons why one should start by analyzing a single bubble as an isolated entity.[11,14] On the one hand, technology has allowed us to experimentally study isolated bubbles in so-called acoustic traps. On the other hand, the knowledge of single-bubble cases facilitates understanding and describing interactions among bubbles, systems consisting of several bubbles, or bubbly liquids. In this work, we also focus on the case of a single bubble, which we deem to be the first step toward multi-bubble systems.[23–27]

In particular, in these pages, we attempt to understand the factors that influence the behavior of a gas bubble in the regime of small-amplitude oscillations. In other words, we look for the essential ingredients for building a good model. It is well known that bubble dynamics goes beyond linear theory and that effects such as sonoluminescence, appearance of chaos, rectified diffusion, or resonances cannot be correctly interpreted without resorting to nonlinearity.[14] However, before moving on to those cases, which will be the subject of future works, it is necessary to clarify which phenomena are already observable in a linear regime and what characteristics a model must have to describe them properly. It should also be emphasized that bubbly liquids are often studied for small-amplitude bubble oscillations.[23,24] Therefore, what is going to be presented here can easily be extended to the study of such physical systems.

In this regard, we will focus on modeling the gas dynamics within the bubble to demonstrate how the former affects the evolution of the

© Author(s) 2025

latter. The hyperbolic systems of balance laws of rational extended thermodynamics (henceforth RET) were introduced to describe phenomena involving gases in conditions far from equilibrium or undergoing very sudden changes.[28,29] We will refer to these theories as a tool that can be naturally employed even in nonlinear regimes of large oscillations,[30–32] although here we test their validity in the linear case. In what follows, we will also compare the approach based on RET with one based on the Navier–Stokes–Fourier (NSF) approximation commonly employed in the literature. The main differences are immediately apparent both in the nature of the partial differential equation systems (parabolicity for NSF vs hyperbolicity for RET) and in the fact that RET treats as independent field variables also non-equilibrium quantities (such as heat flux, dynamic pressure, and deviatoric part of the stress tensor). In this way, the typical NSF constitutive relations are replaced by balance laws.

In the following sections, after recalling which equations are commonly used for the dynamics of a spherical bubble (Sec. II) and briefly introducing the RET theory (Sec. III), we will move on to deal with the role played by different physical elements, as summarized in Sec. IV.

In Sec. V, we will start from thermal effects, finding results already known in the literature.[14,33] We will then investigate the possible action of viscosity by referring to a recent work that investigates the impact of high values of bulk viscosity[32] (Sec. VI) and by verifying whether it is reasonable to neglect the deviatoric part of the stress tensor (Sec. VIII). A first perspective on the role of geometry will be provided in Sec. VII, starting from oversimplified models of non-spherical bubbles.

The delicate issue of boundary conditions at the gas-liquid interface will be addressed in Secs. V and VI in the case of mass conservation, while Secs. X and XI will consider, respectively, gas transfer and the presence of a shell as in ultrasound contrast agents. Section IX will also highlight the advantages and limitations of using a homobaric model, i.e., a set of gas equations derived under the assumption of spatially homogeneous pressure.

Some examples shown in the figures in the following sections (V–XII) will help us understand how some effects become negligible or significant depending on the external conditions and gas properties. For instance, it should be recalled that small bubbles amplify the impact of thermal conductivity, dynamic pressure, geometry, or gas diffusion in the liquid. Conversely, it is known that as the bubble size increases, some modeling aspects become negligible. The role of surfactants and viscoelastic materials is taken into account in Sec. XII, while conclusions are available in Sec. XIII. All the figures we will present were created using ©Matlab

II. ABOUT MODELS OF A GAS BUBBLE IN A LIQUID

In this section, we focus on the case of a single gas bubble immersed in a liquid in the presence of a periodic acoustic driving pressure. We will also assume that the center of the bubble is stationary and the vessel's walls are sufficiently far away.

Bubbles of the most varied forms can be observed in nature and in the laboratory, and sometimes, the only way to describe their evolution over time is through numerical integration. In other cases, a simpler shape or a simplified model allows the derivation of an explicit equation capable of predicting the behavior of the bubble. The most studied bubble shape is the spherical one, due to its simplicity and physical-mathematical symmetry. As a matter of fact, in many instances, there is experimental and theoretical evidence that sphericity is a reasonable assumption. The evolution of a spherical bubble in the presence of an acoustic forcing is commonly ruled by an ordinary differential equation (ODE) for the unknown function $R(t)$, i.e., the radius of the bubble as time varies. The initial idea of introducing such a relationship is due to Lord Rayleigh.[1] Thanks also to the improvements suggested by Plesset,[2] the Rayleigh–Plesset equation has been widely used and is still employed today for simulations of spherical bubbles. It can be written as

$$R\ddot{R}+\frac{3}{2}\dot{R}^2=\frac{1}{\rho_L}p_L,\qquad \text{with}\quad p_L=p_G(R,t)-p_0-p_a(t)-\frac{2\sigma_L}{R}-\frac{4\mu_L\dot{R}}{R}, \tag{1}$$

where $\dot{}$ indicates the time derivative, while p_L represents the difference between the pressure of the liquid on bubble wall $[p_G(R,t)-2\sigma_L/R-4\mu_L\dot{R}/R]$ and the external pressure applied to the liquid. The latter includes both the periodic acoustic forcing $p_a=P_{a0}\sin(\omega t)$ with amplitude P_{a0} and pulsation ω, and the hydrostatic pressure of the liquid p_0. Furthermore, the symbol ρ_L indicates the mass density of the liquid, $p_G(R,t)$ denotes the pressure of the gas on the bubble wall, σ_L and μ_L are the interfacial superficial tension and the viscosity of the liquid, respectively. This first model, however, neglects the compressibility of the liquid and the effects of sound radiation. To overcome the limitations of the theory, first Gilmore[34] and then Keller and Miksis[35] worked on introducing more complete equations. Since the Keller–Miksis equation is notoriously rather complicated, it is often accompanied by a first-order Taylor expansion for the parameter $1/c_L$ considered sufficiently small (c_L denotes the speed of sound in the liquid). In this way, such an approximated ODE can be written as[14]

$$\left(1-\frac{\dot{R}}{c_L}\right)R\ddot{R}+\frac{3}{2}\left(1-\frac{\dot{R}}{3c_L}\right)\dot{R}^2=\left(1+\frac{\dot{R}}{c_L}\right)\frac{1}{\rho_L}p_L+\frac{R}{\rho_L c_L}\frac{dp_L}{dt}. \tag{2}$$

The study of models aimed at describing the behavior of the bubble radius in an increasingly accurate and general manner has continued to this day: we recall, for example, a couple of recent works.[16,36] The analysis has also been generalized to bubbles with different geometries (see Sec. VII for some examples and more details) and extended to bubbles in viscous media or soft tissues or even encapsulated by a lipid coat (we will briefly address this topic in Secs. XI and XII).

Although they almost always have a simple structure, all evolution equations for the bubble radius/volume are affected by a closure problem: in fact, the gas pressure inside the bubble is usually unknown and has to be somehow prescribed. Most publications in the literature overcome this problem by imposing that there be an inverse proportionality between p_G (supposed to be uniform within the bubble) and R, governed by the so-called polytropic process with exponent or index κ[7,14]

$$p_G=p_{GE}(R_0/R)^{3\kappa}\quad\text{with}\quad p_{GE}=p_0+2\frac{\sigma_L}{R_0}=p_0(1+w), \tag{3}$$

where $w=2\sigma_L/(R_0p_0)$, while p_{GE} and R_0, respectively, indicate gas pressure and radius at equilibrium, that is to say,, in the absence of acoustic driving pressure. The *polytropic index* κ is commonly assigned the value 1 in the isothermal regime (this traditionally corresponds to slow oscillations of the bubble) or the value γ, given by the ratio of specific heats, in the adiabatic regime (when the bubble oscillation period turns out to be much smaller than the other time scales involved).

A more precise but much more expensive closure method consists of coupling the ODE for R with a set of equations describing the

10 January 2026 08:22:20

© Author(s) 2025

gas dynamics inside the bubble: these usually range from Euler equations for a gas with no viscosity and no thermal conductivity to classical NSF models.[14,33,37]

In the presence of an acoustic driving pressure, the ODEs that rule the evolution of the bubble radius exhibit the typical structure of a damped and forced nonlinear oscillator. Therefore, all the effects observed and studied in the framework of the dynamics of a spherical bubble can be traced back to the different regimes associated with this model. The parameters that most influence the bubble behavior are the amplitude and angular frequency of the acoustic forcing, the equilibrium radius, and the gas pressure at equilibrium. Here, we will deal with small-amplitude oscillations, using P_{a0} as the perturbation parameter. For this reason, only the effects of ω, R_0, and p_{GE} will be explored. Thus, in what follows, we will assume the amplitude of the sound signal acting on the liquid to be very small ($P_{a0} = p_{GE}\varepsilon$ with $\varepsilon \ll 1$). Consequently, the response of all the physical quantities involved will be equally small. Under these conditions, the bubble radius can be expressed as $R = R_0(1 + X_1)$ (where $|X_1| \ll 1$) and the equation describing the behavior of X_1 will be obtained by linearizing the one that governs the dynamics of R. Historically, linearized gas pressure is described as the sum of two terms besides p_{GE}: one associated with the polytropic index, the other with a damping constant μ_G

$$p_G(R_0, t) = p_{GE} + p_0 p_{G1} = p_{GE} - 3\kappa p_{GE} X_1 - 4\mu_G \dot{X}_1. \tag{4}$$

In a linear regime, the term $-3\kappa p_{GE} X_1$ can be easily deduced by referring to a polytropic process. If gas dynamics is described by either the NSF or the RET equations, the quantity $-4\mu_G \dot{X}_1$ (originally suggested by Prosperetti[38]) should also be introduced to take into account any dissipative effects (as thermal or viscosity ones) that can give rise to a damping phenomenon in bubble dynamics. In the following sections (V–X), we will determine μ_G for different models and conditions, verifying the reasonableness of (4).

By referring to (2) and (4) (i.e., taking into account also radiation pressure) and introducing a complex representation, the linearized equation for X_1 becomes

$$\ddot{X}_1 + \left(4\frac{\mu_L + \mu_G}{\rho_L R_0^2} + \frac{\omega^2 R_0/c_L}{1 + \dfrac{\omega^2 R_0^2}{c_L^2}}\right)\dot{X}_1 + \left(3\kappa\frac{p_{GE}}{\rho_L R_0^2} - \frac{2\sigma_L}{\rho_L R_0^3} + \frac{\omega^4 R_0^2/c_L^2}{1 + \dfrac{\omega^2 R_0^2}{c_L^2}}\right) X_1 = -\frac{p_0 \varepsilon}{\rho_L R_0^2}\exp(i\omega t). \tag{5}$$

Comparison of (5) with the typical equation of a damped and forced linear oscillator[7,33] written in the notation

$$\ddot{X}_1 + 2\beta_{tot}\dot{X}_1 + \omega_0^2 X_1 = -\frac{p_0 \varepsilon}{\rho_L R_0^2}\exp(i\omega t), \tag{6}$$

allows the identification of damping coefficients β_{tot} and natural angular frequency[39] ω_0. In fact, it holds[33]

$$\begin{aligned} &\beta_{tot} = \beta_L + \beta_G + \beta_{ac}, \\ &\text{with} \quad \beta_L = \frac{2\mu_L}{\rho_L R_0^2}, \quad \beta_G = \frac{2\mu_G}{\rho_L R_0^2}, \quad \beta_{ac} = \frac{1}{2}\frac{\omega^2 R_0/c_L}{1 + \dfrac{\omega^2 R_0^2}{c_L^2}}, \\ &\omega_0^2 = 3\kappa\frac{p_{GE}}{\rho_L R_0^2} - \frac{2\sigma_L}{\rho_L R_0^3} + \frac{\omega^4 R_0^2/c_L^2}{1 + \dfrac{\omega^2 R_0^2}{c_L^2}}, \end{aligned} \tag{7}$$

where three different damping coefficients are described: β_L is associated with the viscous effects of the liquid, β_G is due to any dissipation effects in the gas, and the coefficient β_{ac} takes into account the acoustic effects observable only for high pulsations and sufficiently large bubbles.[33] Moreover, we note that for a monatomic gas β_G is only due to thermal effects (both in NSF and RET models) and is dominant with respect to β_L and β_{ac} as R_0 increases and the values of ω are not very high.[33,38] In the polyatomic case, β_G is also affected by bulk viscosity, thus giving rise to two different phenomena. For large bubbles, thermal effects still dominate, as in the monatomic case, and RET and NSF predict identical results. For small bubbles ($R_0 \lesssim 10^{-5}$ m), however, the role of high bulk viscosity becomes prominent and β_G may again exceed β_L and β_{ac}, while the predictions of RET and NSF show significant discrepancies (see Secs. V and VI). Similar considerations also apply to κ.

It should be noted that β_{tot} and ω_0^2 produce observable effects on the bubble's steady-state oscillations, since they are associated with phase shift and resonance phenomena commonly studied in experiments.[3] For this reason, in what follows, we will focus on the coefficient κ and β_G, strictly related to natural angular frequency and damping coefficient.

III. A BRIEF PRESENTATION OF RATIONAL EXTENDED THERMODYNAMICS THEORIES

In this section, we go beyond the traditional NSF description of the gas inside the bubble for two reasons. On the one hand, it is well known that NSF constitutive relations can be obtained from RET as a limit for small relaxation times[28,29] through a technique known as Maxwellian iteration.[40] This implies that RET can capture effects that NSF cannot optimally describe when relaxation times are not so small compared to other time scales of the physical system. Thus, differences between the two theories can be observed even in a linear regime, as we will also verify in the following sections (VI–XII). On the other hand, this work represents the first testbed of RET for future nonlinear applications, where the hyperbolic nature of its partial differential equation (PDE) systems, combined with the presence of dissipative terms, makes the description of far-from-equilibrium phenomena and possible shock formations more realistic (both with respect to NSF and Euler models[28–30]). In this regard, the results obtained here could also be used to test and validate numerical methods.

RET arises from the need to describe phenomena in conditions far from thermodynamic equilibrium in a mathematically and physically correct and accurate manner. To overcome the well-known paradox of infinite velocities intrinsically linked to parabolic systems of PDEs, it is necessary to switch to hyperbolic PDEs. The final result of the work of Müller, Ruggeri, and co-workers[28] is precisely the construction of sets of balance laws for monatomic gases, that are associated with a convex entropy and can be rewritten in hyperbolic symmetric form if the main field variables[28,29] are considered. Thus, the well-posedness of Cauchy problems is guaranteed.[28] After some significant results[28] (e.g., in shock structures, light scattering, dispersion of sound, second sound), the theory was successfully adapted to the case of polyatomic gases by Arima *et al.*,[41] taking into account the rotational and vibrational degrees of freedom of the molecules. In this case, too, very promising results were obtained, in agreement with experimental data.[29] The elegance of RET theories lies in the fact that it is possible to construct this type of model using different approaches, yet obtaining coincident results. On the one hand, at the

10 January 2026 08:22:20

© Author(s) 2025

phenomenological level, it is possible to impose that the set of equations be compatible with the principles of physics (Galilean theory in the classical case, the entropy principle, the principle of material indifference, etc.).[28,29,41] On the other hand, the method of moments applied to the Boltzmann equation of kinetic theory allows us to construct one or more infinite hierarchies of moments (it is known that in the polyatomic case these hierarchies are at least two[42]) which are then truncated at a certain number of moments and closed through the maximum entropy principle.[28,29]

To give a rough idea of the procedure, let us consider the polyatomic case, starting from the Boltzmann equation (if t time, c_j jth component of the microscopic velocity, z_j jth coordinate, $\partial_t = \partial/\partial t$, $\partial_{z_j} = \partial/\partial z_j$)

$$\partial_t f + \sum_{j=1}^{3} c_j \partial_{z_j} f = \mathscr{Q} \tag{8}$$

which has the same form as the well-known monatomic case, except for the structure of collisional terms $\mathscr{Q}$ and for the dependence of the probability density function f. In fact, it holds that $f = f(t, \mathbf{z}, \mathbf{c}, I)$,[43] that is, in addition to depending on the usual variables t, $\mathbf{z} = (z_1, z_2, z_3)$ and $\mathbf{c} = (c_1, c_2, c_3)$, it is also a function of the non-negative scalar quantity I representing the internal molecular modes. Two hierarchies of moments akin to

$$\partial_t \mathbf{F} + \partial_{z_k} \mathbf{F}^k = \mathbf{Q}, \quad \partial_t \mathbf{G}_{ll} + \partial_{z_k} \mathbf{G}^k_{ll} = \mathbf{Q}_{ll}, \tag{9}$$

can be derived starting from the definitions of F-moments [with densities $\mathbf{F} = (F, F_{i_1}, F_{i_1 i_2}, F_{i_1 i_2 i_3}, \ldots)$ and fluxes $\mathbf{F}^k = (F_k, F_{ki_1}, F_{ki_1 i_2}, F_{ki_1 i_2 i_3}, \ldots)$]

$$\begin{aligned} F &= m \int_{\mathbb{R}^3} \int_{\mathbb{R}^+} f \varphi(I) dI d\mathbf{c}, \\ F_{i_1 i_2 \ldots i_n} &= m \int_{\mathbb{R}^3} \int_{\mathbb{R}^+} f \varphi(I) c_{i_1} c_{i_2} \ldots c_{i_n} dI d\mathbf{c}, \end{aligned} \tag{10}$$

and G-moments [with densities $\mathbf{G}_{ll} = (G_{ll}, G_{lli_1}, G_{lli_1 i_2}, G_{lli_1 i_2 i_3}, \ldots)$ and fluxes $\mathbf{G}^k_{ll} = (G_{llk}, G_{llki_1}, G_{lki_1 i_2}, G_{llki_1 i_2 i_3}, \ldots)$], given by

$$\begin{aligned} G_{ll} &= \int_{\mathbb{R}^3} \int_{\mathbb{R}^+} f (mc^2 + 2I) \varphi(I) dI d\mathbf{c} \\ G_{lli_1 i_2 \ldots i_n} &= m \int_{\mathbb{R}^3} \int_{\mathbb{R}^+} f (mc^2 + 2I) \varphi(I) c_{i_1} c_{i_2} \ldots c_{i_n} dI d\mathbf{c}, \end{aligned} \tag{11}$$

if $l, k, i_j \in \{1, 2, 3\}$ and $j, n \in \mathbb{N} \backslash \{0\}$, m denoting the molecular mass. The weighting measure $\varphi(I)$ is defined based on the gas properties, or more precisely, on its equilibrium caloric state equation. The production terms represented by the vectors $\mathbf{Q}$ and $\mathbf{Q}_{ll}$ are always calculated using the moment method starting from the collisional terms and, in order to be consistent with the physics of the system, also involve the conservation of mass, momentum, and energy (hence the zero components)

$$\mathbf{Q} = (0, 0_{i_1}, Q_{i_1 i_2}, \ldots), \quad \mathbf{Q}_{ll} = (0, Q_{lli_1}, Q_{lli_1 i_2}, \ldots). \tag{12}$$

Now, the infinite hierarchies, once truncated by a given number of moments (the choice of this number is not entirely arbitrary[29,42]) must be closed. In other words, it is necessary to express all the production terms and the final fluxes as functions of the densities. The maximum entropy principle is the tool employed for this purpose, and after several calculations, some additional assumptions related to convergence problems, and the Taylor expansion in the neighborhood of an equilibrium state for the non-equilibrium variables, the desired system of equations is obtained. In this work, we will refer to the 14-moment model linearized in the non-equilibrium variables, since it is the simplest RET model for polyatomic gases that takes heat flux into account. In this case, we start from the moments $\mathbf{F} = (F, F_{i_1}, F_{i_1 i_2})$ and $\mathbf{G}_{ll} = (G_{ll}, G_{lli_1})$, arriving at a set of 14 PDEs for the 14 independent field variables: mass density ρ, gas velocity $\mathbf{v}$, equilibrium pressure p, deviatoric part of the stress tensor $\sigma_{\langle ij \rangle}$ (with i and $j \in \{1, 2, 3\}$), dynamic pressure Π, and heat flux $\mathbf{q}$. We assume that we are dealing with an ideal, polytropic gas, that is, we impose the following thermal and caloric state equations:

$$p = \frac{k_B \rho T}{m}, \quad e = c_V T = \frac{D k_B T}{2m}, \tag{13}$$

where e denotes the specific internal energy, k_B the Boltzmann constant, c_V the specific heat at constant volume and D the molecular degrees of freedom with $D \geq 3$. Then the 14-moment system in Cartesian coordinates is comprised of the conservation laws of mass, momentum, and energy

$$\begin{aligned} &\partial_t \rho + \partial_{z_l}(\rho v_l) = 0, \\ &\partial_t(\rho v_i) + \partial_{z_k}(\rho v_i v_k + p\delta_{ik} - \sigma_{ik}) = 0 \\ &\partial_t(\rho v^2 + 2\hat{c}_V p) + \partial_{z_k}\left[\rho v^2 v_k + 2(\hat{c}_V + 1) p v_k - 2\sigma_{lk} v_l + 2q_k\right] = 0, \end{aligned} \tag{14}$$

and of the following balance laws:

$$\begin{aligned} &\partial_t(\rho v_i v_j + p\delta_{ij} - \sigma_{ij}) + \partial_{z_k}\Big[\rho v_i v_j v_k + p(v_i \delta_{jk} + v_j \delta_{ik} \\ &\quad + v_k \delta_{ij}) - \sigma_{jk} v_i - \sigma_{ik} v_j - \sigma_{ij} v_k + \frac{q_i \delta_{jk} + q_j \delta_{ik} + q_K \delta_{ij}}{\hat{c}_v + 1}\Big] \\ &\quad = -\frac{\Pi \delta_{ij}}{\tau_\Pi} + \frac{\sigma_{\langle ij \rangle}}{\tau_\sigma}, \\ &\partial_t(\rho v^2 v_i + 2((\hat{c}_v + 1) p v_i - \sigma_{il} v_l + q_i)) \\ &\quad + \partial_{z_k}\Big[\rho v^2 v_i v_k + p(v^2 \delta_{ik} + 2(\hat{c}_V + 2) v_i v_k) - \sigma_{ik} v^2 - 2\sigma_{il} v_l v_k \\ &\quad - 2\sigma_{kl} v_l v_i + 2(\hat{c}_V + 1)^{-1} q_l v_l \delta_{ik} + 2(1 + (\hat{c}_V + 1)^{-1}) \\ &\quad \times (q_i v_k + q_k v_i) + 2\frac{p}{\rho}\left((\hat{c}_V + 1) p \delta_{ik} - (\hat{c}_V + 2)\sigma_{ik}\right)\Big] \\ &\quad = -\frac{2q_i}{\tau_q} - 2\left(\frac{\Pi \delta_{il}}{\tau_\Pi} + \frac{\sigma_{\langle il \rangle}}{\tau_\sigma}\right) v_l. \end{aligned} \tag{15}$$

Regarding the notation adopted in (14) and (15), some clarifications are needed: first of all, from now on, we will imply a summation over repeated indices (for example, $q_l v_l$ has to be understood as $\sum_{l=1}^{3} q_l v_l$), then for the sake of compactness, we have introduced the viscous stress tensor $\sigma_{ik} = \sigma_{\langle ik \rangle} - \Pi \delta_{ik}$ and the quantity $\hat{c}_V = c_V m / k_B$. Finally, the relaxation times related to $\sigma_{\langle ij \rangle}$, Π and q_i are proportional to the measurable physical parameters *shear viscosity* μ_s, *bulk viscosity* μ_b and *heat conductivity* k_G, from the relations

$$\tau_q = \frac{2 k_G m}{(D + 2) k_B p}, \quad \tau_\sigma = \frac{\mu_s}{p}, \quad \tau_\Pi = \frac{3D\mu_b}{2(D - 3)p}. \tag{16}$$

It is possible to prove[44] that the system comprised of (14) and (15) satisfies the hyperbolic requirements in a region of phase space that also

10 January 2026 08:22:20

© Author(s) 2025

includes the equilibrium state. Moreover, it should be recalled that Eqs. (14) and (15) are also valid in the case of a monatomic gas: in that limit, it holds $D = 3$ and $\Pi = 0$, and the system is reduced to the well-known 13-moment Grad's model.[29]

In the following sections (V–XII), we will deal with problems in planar, cylindrical, and spherical symmetry. For this reason, we will rewrite the previous equations in these three geometries, assuming that all field variables depend on a single coordinate, which we will denote by z. This coordinate has the meaning of the first component z_1 of the Cartesian coordinates in the planar case, while it represents the radial coordinate r in both the cylindrical and spherical frameworks. To compact the formulas, we introduce the geometric parameter N, with $N = 1$ in the planar case, $N = 2$ in the cylindrical one, and $N = 3$ in the spherical one. Finally, to simplify the calculations, we will not refer to the covariant or contravariant components for vectors and tensors: instead, we will introduce the physical components as proposed by Truesdell,[45] starting from the metric tensor g_{ij}

$$\tilde{v}^h = \sqrt{g_{\underline{hh}}}v^h, \quad \tilde{q}^h = \sqrt{g_{\underline{hh}}}q^h, \quad \tilde{\sigma}^{\langle hk\rangle} = \sqrt{g_{\underline{ii}}g_{\underline{jj}}}\sigma^{\langle hk\rangle}; \tag{17}$$

in this instance, the repeated indices are not added and are therefore underlined. Thanks to the physical assumptions about the symmetry of the problem, the only non-zero component of velocity and heat flux vectors will be the first one, and for brevity, we will indicate it as

$$v = \tilde{v}^1, \quad q = \tilde{q}^1.$$

The same symmetry condition implies that $\tilde{\sigma}^{\langle hk\rangle} = 0$ if $h \neq k$. Finally, we will omit the supersign $\tilde{}$ when referring to the non-zero components of the tensor, that is, those with the same value of the two indices, since from now on we will only consider physical components, and therefore no confusion can arise. Having introduced the material derivative (for example, for the quantity u, $\dot{u} = \partial_t u + v\partial_z u$) we can write (14) and (15) in the form (with $\sigma^{11} = \sigma^{\langle 11\rangle} - \Pi$)

$$\begin{aligned}
&\dot{\rho} + \rho\frac{1}{z^{N-1}}\partial_z(z^{N-1}v) = 0,\\
&\dot{v} - \frac{1}{\rho}\partial_z\sigma^{\langle 11\rangle} + \frac{1}{\rho}\partial_z\Pi + \frac{1}{\rho}\partial_z p = \mathcal{Q}_2,\\
&\dot{\sigma}^{\langle 11\rangle} + \frac{7\sigma^{\langle 11\rangle} - 4(p+\Pi)}{3}\partial_z v - \frac{8}{3(D+2)}\partial_z q = \mathcal{Q}_3,\\
&\dot{\Pi} + \left[\Pi - \frac{2(D-3)(\sigma^{11}-p)}{3D}\right]\partial_z v + \frac{4(D-3)}{3D(D+2)}\frac{1}{z^{N-1}}\partial_z\left(z^{N-1}q\right) = \mathcal{Q}_4,\\
&\dot{\rho} + \left[p + \frac{2(p-\sigma^{11})}{D}\right]\partial_z v + \frac{2}{D}\partial_z q = \mathcal{Q}_5,\\
&\dot{q} + \frac{p}{2\rho^2}\left[2\sigma^{11} - (D+2)\left(p-\sigma^{11}\right)\right]\partial_z\rho + \frac{2(D+5)q}{D+2}\partial_z v\\
&\quad - \frac{\sigma^{11}+p}{\rho}\left(\partial_z\sigma^{\langle 11\rangle} - \partial_z\Pi\right) + \frac{(D+2)(p-\sigma^{11})}{2\rho}\partial_z p = \mathcal{Q}_6,\\
&\dot{\sigma}^{\langle 22\rangle} + \left[\frac{2}{3}\left(p + \Pi - \sigma^{\langle 11\rangle}\right) + \sigma^{\langle 22\rangle}\right]\partial_z v + \frac{4}{3(D+2)}\partial_z q = \mathcal{Q}_7,
\end{aligned} \tag{18}$$

where

$$\begin{aligned}
\mathcal{Q}_2 &= (N-1)\frac{(\sigma^{\langle 11\rangle} - \sigma^{\langle 22\rangle})}{z\rho},\\
\mathcal{Q}_3 &= -\frac{\sigma^{\langle 11\rangle}}{\tau_\sigma} - \frac{4(N-1)q}{3(D+2)z} - \frac{(N-1)v}{3z}\\
&\quad \times\left[2(p+\Pi+\sigma^{\langle 11\rangle} - -2\sigma^{\langle 22\rangle}) + (N-1)(\sigma^{\langle 11\rangle} + 2\sigma^{\langle 22\rangle})\right],\\
\mathcal{Q}_4 &= -\frac{\Pi}{\tau_\Pi} - \frac{(N-1)v}{3Dz}\Big[6(\sigma^{\langle 22\rangle} - p - \Pi) + D\big(-\sigma^{\langle 11\rangle} - -4\sigma^{\langle 22\rangle}\\
&\quad + 5\Pi + 2p + (N-1)v(\sigma^{\langle 11\rangle} + 2\sigma^{\langle 22\rangle})\big)\Big],\\
\mathcal{Q}_5 &= -(N-1)\left[2\frac{q}{Dz} + 2\frac{(p+\Pi-\sigma^{\langle 22\rangle})v}{Dz} + \frac{pv}{z}\right],\\
\mathcal{Q}_6 &= -\frac{q}{\tau_q} - \frac{(N-1)}{z}\left[\frac{(\sigma^{\langle 22\rangle} - \sigma^{\langle 11\rangle})(p+\sigma^{11})}{\rho} + \frac{(D+4)qv}{D+2}\right],\\
\mathcal{Q}_7 &= -\frac{\sigma^{\langle 22\rangle}}{\tau_\sigma} - (N-1)\frac{2(3(N-1)-7)q}{3(D+2)z} - \frac{(N-1)v}{3z}\\
&\quad \times\Big[8\sigma^{\langle 22\rangle} - \sigma^{\langle 11\rangle} - 7p - 7\Pi + (N-1)\\
&\quad \times(3p + 3\Pi + \sigma^{\langle 11\rangle} - \sigma^{\langle 22\rangle})\Big].
\end{aligned} \tag{19}$$

Before starting to model the gas inside the bubble using the equations we have just written, it is important to underline again that unlike the classical approach of the Navier–Stokes–Fourier model, in (15) or (18) even the non-equilibrium variables—namely, the deviatoric part of the stress tensor, the dynamic pressure, and the heat flux—are independent variables, subject to balance laws.

IV. WHAT TO INCLUDE OR NEGLECT IN A LINEAR MODEL OF BUBBLE OSCILLATIONS

Although many effects are typical expressions of nonlinearity, it is not always clear which elements affect bubble description, even in the regime of small-amplitude oscillations. In the following sections (V–XII), we attempt to investigate several modeling aspects related to the gas inside the bubble, to the gas–liquid interface, to the geometry, and to the features of the equations. The aim is not to provide a comprehensive discussion (which would be impossible, after all), but instead to identify key points and test the reasonableness of some hypotheses commonly introduced in the literature.

To assess the relevance of the elements to be analyzed, we will focus on the determination of the polytropic index κ and damping coefficient β_G [see (4) and (7)]. Note that here, we will not assume that the values of these parameters are known *a priori*. An *a posteriori* analysis of the results could guide the choice of the values of these quantities in the future, when opting for the hypothesis (3), even in nonlinear regimes.

To describe the gas dynamics in a bubble, we will refer to RET equations, ignoring models that differ only in nonlinear terms, such as equations for non-polytropic gases,[29] or RET theories with Taylor expansion in non-equilibrium variables at second or higher order.[28,29,44]

Regarding the modeling of the gas–liquid interface, or possibly gas–shell interface, we will compare different boundary conditions. Gas diffusion requires a separate discussion: in a bubble, this phenomenon is always associated with nonlinear effects such as rectified diffusion. Here, the purpose will be to offer a first perspective on this

10 January 2026 08:22:20

© Author(s) 2025

aspect, despite the major limitations of a linear approach. Effects due to the presence of other bubbles or to the proximity of the walls of the vessel containing the liquid will not be taken into account, as they are not significant in the case of small amplitude oscillations.

Using highly simplified models, we will also attempt to analyze the impact of bubble geometry. This is a preliminary investigation, since more complex geometric symmetries would require a numerical approach and the addition of nonlinear terms, which we will ignore here.

In all these cases, we will verify that both κ and β_G do not depend on the type of equation chosen to describe the dynamics of the bubble radius/volume, except for the surface tension term. This result is clearly a consequence of linearization, since predictions of nonlinear phenomena show a significant dependence on the model chosen to describe the evolution of bubble walls.

As for the equilibrium hydrostatic pressure of the liquid p_0 and its equilibrium temperature T_0, we will limit ourselves to considering standard environmental conditions. Unless otherwise noted, the examples shown in the figures below refer to a gas bubble immersed in water at a temperature $T_0 = 300\,\mathrm{K}$ and an ambient pressure $p_0 = 10^5\,\mathrm{Pa}$.

A. Time scales and bubble dynamics

Referring to the RET model presented in Sec. III [see, for example, (18) and (19)] and taking into account bubble dynamics, it is possible to identify several time scales, which, as we will see, assume different roles depending on the prescribed physical conditions. In fact, in addition to the three relaxation times associated with the non-equilibrium variables (16), the periodic acoustic forcing naturally introduces an additional timescale, inversely proportional to its angular frequency ($t_\omega = \omega^{-1}$). Finally, another characteristic time must be taken into account: that is, the time it takes sound to travel from the center to the wall of the bubble, which is proportional to $t_0 = R_0/\sqrt{k_B T_0/m}$. In the following analysis, we will show how the dimensionless number $r_t = t_0/t_\omega$, or better yet, its square[32]

$$r_t^2 = \left(\frac{t_0}{t_\omega}\right)^2 = \frac{R_0^2\omega^2 m}{k_B T_0} = \frac{\omega^2 R_0^2 \rho_0}{p_0(1+w)}, \tag{20}$$

can be a reference for distinguishing different regimes, even in a linear approximation (ρ_0 is the mass density of the gas at equilibrium). We stress that r_t represents both a ratio of time scales (hence t as a subscript) but also of spatial scales, since it is proportional to the ratio between the equilibrium bubble radius and the wavelength of the acoustic signal in the gas.

Thus, when $r_t \ll 1$, the time needed for a signal to cross the bubble is significantly less than the oscillation period, or equivalently, the wavelength is greater than the radius of the bubble: this implies that the temperature of the gas remains constantly equal to that of the bubble wall, and an isothermal behavior of the gas can be observed. Conversely, values of $r_t \simeq 1$ are associated with nearly adiabatic regimes, since a signal does not have enough time to cross the bubble before the oscillation is completed. In this regard, however, one must also take into account homabaricity. As we will show in Sec. IX, when $r_t^2 > 1$ the gas pressure in the bubble is no longer uniform in space; that is to say, the homobaric assumption fails, and instabilities could appear that lead to the dissolution of the bubble itself.[7,33]

In what follows, we will compare the other characteristic times with t_ω: for this reason, we introduce the dimensionless quantities from (16)

$$\hat{\tau}_q = \tau_q\omega, \quad \hat{\tau}_\sigma = \tau_\sigma\omega, \quad \hat{\tau}_\Pi = \tau_\Pi\omega. \tag{21}$$

If a relaxation time turns out to be small compared to t_ω, the corresponding non-equilibrium field variable relaxes quickly and can be somehow neglected. Conversely, as the dimensionless relaxation time defined in (21) increases, the physical quantity associated with it does not have sufficient time to vanish, and bubble oscillations enhance non-equilibrium effects. Note that condition $r_t^2 \lesssim 1$ limits the range of values of ω that guarantees bubble stability when R_0 and m are assigned. In particular, at room temperature and for a gas like Ar or CO_2, the values that can be taken into consideration for the angular frequency are approximately $\omega \leq 250 R_0^{-1}\,\mathrm{ms}^{-1}$. Thus, $\hat{\tau}_\Pi$ can become dominant in the dynamics of a small bubble, while this does not happen for high values of R_0.

B. Some preliminary definitions

In what follows, we refer to steady-state oscillations. In other words X_1, p_{G1} and all remaining perturbation quantities may be taken to have the same time dependence as the acoustic periodic forcing, so that $\dot{X}_1 = i\omega X_1$, $\dot{p}_{G1} = i\omega p_{G1}$, etc. Thus, under the previous assumption, using the complex representation and taking into account relation (4), it holds

$$\kappa = -\Re\left(\frac{p_0 p_{G1}}{3 p_{GE} X_1}\right), \quad \mu_G = -\Im\left(\frac{p_0 p_{G1}}{4\omega X_1}\right). \tag{22}$$

Furthermore, to simplify notation and steps for writing linearized RET equations, we introduce the following quantities associated with the dimensionless relaxation times in (21):

$$a_q = 1 - i\hat{\tau}_q^{-1}, \quad a_\Pi = 1 - i\hat{\tau}_\Pi^{-1}, \quad a_\sigma = 1 - i\hat{\tau}_\sigma^{-1}. \tag{23}$$

The corresponding quantities in the case of NSF are

$$a_q^{NSF} = -i\hat{\tau}_q^{-1}, \quad a_\Pi^{NSF} = -i\hat{\tau}_\Pi^{-1}, \quad a_\sigma^{NSF} = -i\hat{\tau}_\sigma^{-1}. \tag{24}$$

The differences between definitions (23) and (24) are due to the fact that by moving from RET to NSF, we switch from balance laws to constitutive relations. Finally, to further simplify calculations and results, it is also appropriate to introduce the following dimensionless quantities related to the RET model:

$$J_\Pi = \frac{2(D-3)}{2(D-3) + 3(D+2)a_\Pi}, \quad J_\sigma = -\frac{4D(1-J_\Pi)}{3(D+2)a_\sigma}. \tag{25}$$

In the case of NSF in Sec. VI, the following expression will be used as well:

$$J_\Pi^{NSF} = \frac{2(D-3)}{2(D-3) + 3D a_\Pi^{NSF}}. \tag{26}$$

V. THE ROLE OF THE THERMAL EFFECT: THE CASE OF A MONATOMIC GAS IN A SPHERICAL BUBBLE

The role of the thermal effect in the small-amplitude oscillation regime was extensively studied by Prosperetti in 1977.[33] Here, we résumé his approach to analyze the case of a monatomic gas in a

10 January 2026 08:22:20

© Author(s) 2025

spherical bubble, under the assumption of mass conservation. To this end, for the time being, we ignore the presence of the deviatoric part of the stress tensor (we will return to this point in Sec. VIII) and introduce the field variables linearization in the neighborhood of an equilibrium state [$R_E = R_0$, $\rho_E = \rho_0$, $v_E = 0$, $p_E = p_{GE} = p_0(1+w)$, $q_E = 0$]

$$R = R_0(1+X_1), \quad \rho = \rho_0(1+\rho_{G1}), \quad v = \frac{p_0}{\omega R_0 \rho_0} V_1, \\ p = p_0(1+w+p_1), \quad q = \frac{p_0^2}{\omega R_0 \rho_0} Q_1. \tag{27}$$

As usually done, we replace the spatial variable r with $x = r/R_0 \in [0,1]$ [note that in general it would be appropriate to introduce $y = r/R(t)$, but for the linear regime $x \simeq y$]. Thus, considering Grad's 13-moment model in which $\sigma^{\langle ij \rangle}$ is neglected [i.e., Eq. (18) with (19) when $N = 3$, $D = 3$, $\sigma^{\langle ij \rangle} = \Pi = 0$], we obtain the following relations for the field variables of the gas inside the bubble [referring to (20) and (23)]:

$$\rho_{G1} = i \frac{r_t^{-2}}{1+w} \frac{1}{x^2} \partial_x (x^2 V_1), \\ V_1 = i \partial_x p_1, \\ p_1 = \frac{5}{3} i r_t^{-2} \frac{1}{x^2} \partial_x (x^2 V_1) + \frac{2}{3} i \frac{r_t^{-2}}{1+w} \frac{1}{x^2} \partial_x (x^2 Q_1), \\ Q_1 = \frac{5i}{2} \frac{1+w}{a_q} \left[\partial_x \left(\frac{r_t^{-2}}{x} \partial_{xx}^2 (x p_1) \right) + \partial_x p_1 \right], \tag{28}$$

where, obviously, from (4) $p_1 = p_{G1}$ represents the perturbation of the total gas pressure. By substitution, after a few steps, it is possible to write down an ODE for the gas pressure that has the following general structure (if $\mathscr{P}_1$ is the generic unknown function)

$$\partial_{xxxx}^4 (\mathscr{P}_1 x) + r_t^2 a_2 \partial_{xx}^2 (\mathscr{P}_1 x) + r_t^4 a_0 (\mathscr{P}_1 x) = 0, \tag{29}$$

which, as we will see in the next sections (VI–VII), is typical of small amplitude oscillations for a gas contained in a spherical bubble.

The general solution of (29) (assuming that there is no singularity in the center of the bubble $x = 0$) can therefore be expressed as

$$\mathscr{P}_1 = \sum_{j=1}^{2} A_j \frac{\sinh(\lambda_j r_t x)}{x \sinh(\lambda_j r_t)}, \tag{30}$$

if the characteristic polynomial

$$\lambda^4 + a_2 \lambda^2 + a_0 = 0 \tag{31}$$

is associated with Eq. (29) and its roots are easily identifiable; in particular, we define

$$\lambda_{1,2}(a_2, a_0) = 2^{-1/2} \left(-a_2 \pm \sqrt{a_2^2 - 4a_0} \right)^{1/2}. \tag{32}$$

For a monatomic gas described by the Grad model, we have

$$\mathscr{P}_1 = p_1 = p_{G1}^m, \quad a_2 = a_{2,RET}^m = 1 + a_q, \\ a_0 = a_{0,RET}^m = \frac{3a_q}{5}. \tag{33}$$

Similar calculations can be carried out starting from the NSF model referred to in Ref. 33. In this case, the linearized equations are the same as (28) except for the last equation in which a_q must be replaced by a_q^{NSF} defined in (24).

To determine p_{G1} in the case of the NSF model, one can follow the procedure described in the previous steps: the results turn out to be the same, taking care to substitute a_q for a_q^{NSF} each time.

For the sake of compactness, from now on, both the RET and NSF quantities for a monatomic gas will be denoted by a single notation

$$\lambda_j^m = \lambda_j(a_2^m, a_0^m) \quad j = 1, 2.$$

A. Boundary conditions

The solution of the ODE system that describes small amplitude oscillations contains integration constants (in the present case, the quantity A_j) that are fixed by requiring appropriate boundary conditions at the gas–liquid interface. Since the aim of this work is to study linear phenomena, we will limit ourselves to imposing a couple of different conditions, which will often yield the same results in the cases we studied. Before imposing these conditions and discussing their physical meaning, it is important to dwell on the notation: from now on, the value of the field variables on the wall of the bubble in contact with the liquid will be indicated by $|_b$, so for example, for the generic variable u

$$u|_b = u(r = R, t) = u(x = 1, t). \tag{34}$$

Conservation of mass naturally implies that the velocity of the gas at the bubble wall coincides with the velocity of the wall itself. Taking into account the hypothesis of steady-state oscillations and definitions (20) and (27), the mass conservation condition reduces to

$$v|_b = \dot{R} \quad \Rightarrow \quad V_1|_b = i r_t^2 (1+w) X_1. \tag{35}$$

We refer to Sec. X for the analysis of phenomena involving gas diffusion.

A second condition arises from analyzing the thermal aspects of the problem and can be assigned in different ways. Here, we report two types of conditions that, from now on, we will indicate as *case a* and *case b*.

As we will explicitly verify for monatomic gases, the two thermal conditions we are going to study produce very similar results in all cases of small-amplitude oscillations. Therefore, in what follows, some results will be presented only for *case a*. Obviously, more evident differences between *case a* and *case b* could be observed in highly nonlinear regimes, but this point is beyond the scope of the paper.

In *case a*, the liquid is described as an infinite reservoir at constant temperature T_0. Under this assumption, the gas temperature T_G at the bubble wall is also imposed to be T_0 and starting from the linearization $T_G = T_0(1 + T_{G1})$ for an ideal gas in a linear regime, it must hold $p_0 p_1 = p_0(1+w)(T_{G1} + \rho_{G1})$. Referring to (20) and (27), the *case a* condition can be written as

$$T_G|_b = T_0 \quad \Rightarrow T_{G1}|_b = 0 \Rightarrow \quad p_1|_b = (1+w)\rho_{G1}|_b. \tag{36}$$

In *case b*, the way to assign thermal conditions at the interface is to assume that the liquid is incompressible but not isothermal, so that the

10 January 2026 08:22:20

© Author(s) 2025

PDE of its temperature T_L can be easily deduced. By prescribing the validity of the Fourier constitutive relation, one can write

$$\partial_t T_L + \frac{1}{c_{vL}}\frac{1}{r^2}\partial_r(r^2 q_L) = 0 \quad \text{with} \quad q_L = -k_L \partial_r T_L, \tag{37}$$

where q_L denotes the heat flux of the liquid, while k_L is its *thermal conductivity*. As already done in Ref. 33, it is easy to linearize the previous equations [in the case where $T_L = T_0(1 + T_{L1})$], obtaining the analytical expression of T_{L1}. By imposing that $\lim_{x\to\infty} T_{L1} = 0$ it must hold

$$T_{L1} = A_L \frac{\exp(-\lambda_L(x-1))}{x(1+w)} \quad \text{with} \quad \lambda_L = \sqrt{i\frac{\omega R_0^2 c_{vL}}{k_L}}. \tag{38}$$

Following the idea of Prosperetti,[33] two further conditions are assumed on the interface and correspond to the requirement of continuity of temperature and heat flux. Thus, from (27), (37), and (38), *case b* condition turns out to be

$$\begin{aligned} (T_G - T_L)|_b = 0 \;\Rightarrow\quad & T_{G1}|_b = T_{L1}|_b, \\ (q_G - q_L)|_b = 0 \;\Rightarrow\quad & \frac{p_0^2}{\omega\rho_0} Q_1|_b = -k_L \partial_x T_L|_b. \end{aligned} \tag{39}$$

1. Case a

Referring to (28) and (30), conditions (35) and (36) become

$$\begin{aligned} \sum_{j=1}^{2} A_j f_{3,j} &= r_t^2(1+w)X_1, \\ \sum_{j=1}^{2} A_j \Gamma_j &= 0, \end{aligned} \tag{40}$$

where

$$\Gamma_j = 1 + \lambda_j^2, \quad f_{3,j} = f_{3,j}(\lambda_j) = \lambda_j r_t \coth(\lambda_j r_t) - 1. \tag{41}$$

The solution of the algebraic system (40) can be written as

$$A_1^{a,m} = \frac{\Gamma_2 r_t^2(1+w)X_1}{\Gamma_2 f_{3,1} - \Gamma_1 f_{3,2}}, \quad A_2^{a,m} = -\frac{\Gamma_1 r_t^2(1+w)X_1}{\Gamma_2 f_{3,1} - \Gamma_1 f_{3,2}}, \tag{42}$$

where the apex a reminds us that the results were obtained in *case a*. Thus, from (22), the polytropic index κ, and the term μ_G in *case a* turns out to be

$$\begin{aligned} \kappa^{a,m} &= -\Re\left(\frac{\Gamma_2 - \Gamma_1}{3(f_{3,1}\Gamma_2 - f_{3,2}\Gamma_1)}\right) r_t^2, \\ \mu_G^{a,m} &= -\Im\left(\frac{(\Gamma_2 - \Gamma_1)}{4\omega(f_{3,1}\Gamma_2 - f_{3,2}\Gamma_1)}\right) r_t^2 p_{GE}, \end{aligned} \tag{43}$$

where, for brevity of notation, we have omitted to indicate that all the quantities appearing in the formulas refer to a monatomic gas.

2. Case b

Referring to Eqs. (28), (30), and (38), and taking into account definitions (41), conditions (35) and (39) give rise to the following algebraic system [if $\Omega_L = i(\lambda_L + 1)\frac{2a_q\omega\rho_0 T_0 k_L}{5p_0^2(1+w)^2}$]:

$$\begin{aligned} \sum_{j=1}^{2} A_j f_{3,j} &= r_t^2(1+w)X_1, \\ \sum_{j=1}^{2} A_j \Gamma_j - A_L &= 0, \\ \sum_{j=1}^{2} (A_j \Gamma_j f_{3,j}) + \Omega_L A_L &= 0, \end{aligned} \tag{44}$$

whose solution can be written as

$$\begin{aligned} A_1^{b,m} &= \frac{\Gamma_2(f_{3,2} + \Omega_L)}{(f_{3,1}\Gamma_2 - f_{3,2}\Gamma_1)\Omega_L + f_{3,1}f_{3,2}(\Gamma_2 - \Gamma_1)} r_t^2(1+w)X_1, \\ A_2^{b,m} &= -\frac{\Gamma_1(f_{3,1} + \Omega_L)}{(f_{3,1}\Gamma_2 - f_{3,2}\Gamma_1)\Omega_L + f_{3,1}f_{3,2}(\Gamma_2 - \Gamma_1)} r_t^2(1+w)X_1, \\ A_L &= \frac{\Gamma_1\Gamma_2(f_{3,2} - f_{3,1})}{(f_{3,1}\Gamma_2 - f_{3,2}\Gamma_1)\Omega_L + f_{3,1}f_{3,2}(\Gamma_2 - \Gamma_1)} r_t^2(1+w)X_1. \end{aligned} \tag{45}$$

Taking into account (22), κ and μ_G turn out to be

$$\begin{aligned} \kappa^{b,m} &= -\Re\left(\frac{\Gamma_2(f_{3,2} + \Omega_L) - \Gamma_1(f_{3,1} + \Omega_L)}{3((f_{3,1}\Gamma_2 - f_{3,2}\Gamma_1)\Omega_L + f_{3,1}f_{3,2}(\Gamma_2 - \Gamma_1))}\right) r_t^2, \\ \mu_G^{b,m} &= -\Im\left(\frac{(\Gamma_2(f_{3,2} + \Omega_L) - \Gamma_1(f_{3,1} + \Omega_L))p_{GE}}{4\omega((f_{3,1}\Gamma_2 - f_{3,2}\Gamma_1)\Omega_L + f_{3,1}f_{3,2}(\Gamma_2 - \Gamma_1))}\right) r_t^2, \end{aligned} \tag{46}$$

where, for the sake of brevity, we have omitted to indicate that all the quantities which appear in the formulas refer to the monatomic case. It can be proven that in the limit for $r_t \to 0$ the polytropic index converges to 1 (isothermal condition) for any monatomic gas confined in a spherical bubble, regardless of the prescribed boundary conditions. On the contrary, it is not possible to determine the limit for $r_t \to \infty$, since as r_t increases, we move away from the so-called homobaricity condition and κ presents oscillations (even with negative values).

B. Some examples

Some examples are introduced to briefly discuss the role of physical parameters and establish whether dissimilar models and/or boundary conditions can produce significant differences. Taking into account the linear regime assumption, here and in the following sections, we will calculate the relaxation time associated with the heat flux from (16), supposing $p = p_{GE}$.

In Figs. 1 and 2, we compare the polytropic index as a function of r_t^2 for different monatomic gases, and in particular, for different molecular masses, in the case of $R_0 = 10^{-4}$ m (Fig. 1) and of $R_0 = 10^{-6}$ m (Fig. 2). The comparison between these two figures highlights the role of the bubble equilibrium radius: the smaller R_0, the greater the difference between the polytropic indexes as the value of the molecular mass varies. The same conclusions follow from the comparison between the predictions of the RET and the NSF models and between the effects of boundary conditions for *case a* and *case b*.

In this regard, two extreme examples are reported in Fig. 3 (for radon gas confined in a bubble of radius $R_0 = 10^{-4}$ m) and Fig. 4 (for helium gas confined in a bubble of radius $R_0 = 10^{-6}$ m). In Fig. 3, it is evident that the differences between polytropic indices calculated using different models are really negligible; as a matter of fact, we remark a

10 January 2026 08:22:20

© Author(s) 2025

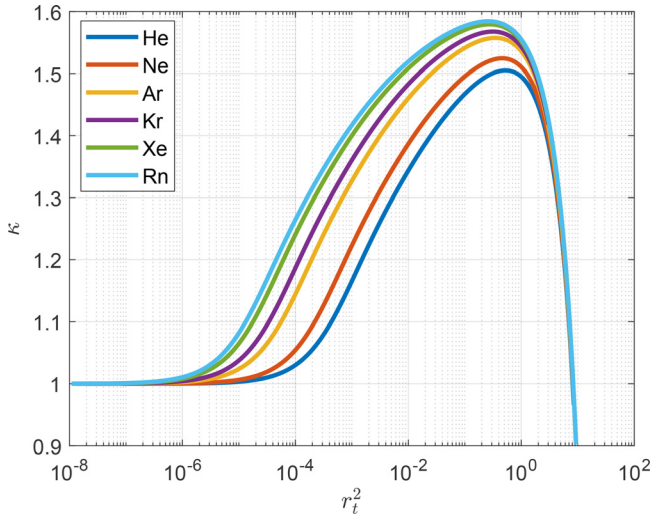

FIG. 1. The polytropic index derived from the RET model, as a function of r_t^2 for different monatomic gases when $R_0 = 10^{-4}$ m and case *a* is imposed.

graphic overlap between the first and second curves. Somewhat more significant differences, although still irrelevant, are due to the prescription of thermal conditions in *case a* and *case b* (third and fourth curves). The presence of a cusp in the graph is due to the use of the absolute value.

The same observations can be made concerning the first two curves in Fig. 4. Imposing different boundary conditions produces similar polytropic index values for large molecular masses and/or large equilibrium radii. However, for small molecular masses and small bubbles (Fig. 4), the values of κ can differ quite significantly when conditions *case a* and *case b* are imposed. A graphical overlap between the curves corresponding to $|\kappa_{RET}^{a,m} - \kappa_{RET}^{b,m}|$ and $|\kappa_{NSF}^{a,m} - \kappa_{NSF}^{b,m}|$ is also present here.

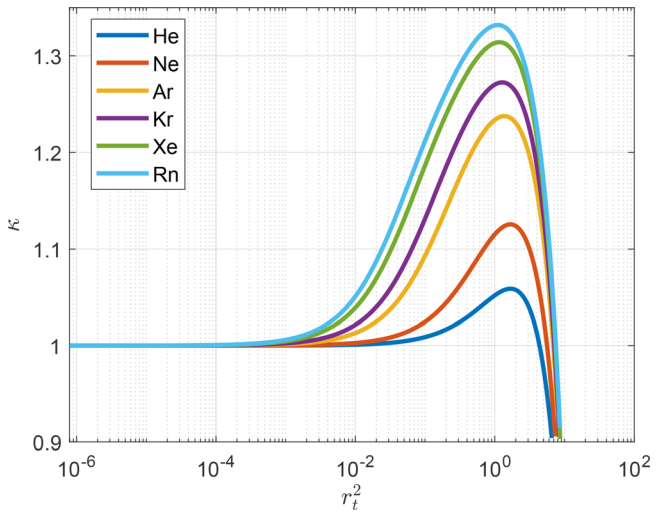

FIG. 2. The polytropic index derived from the RET model, as a function of r_t^2 for different monatomic gases when $R_0 = 10^{-6}$ m and case *a* is prescribed.

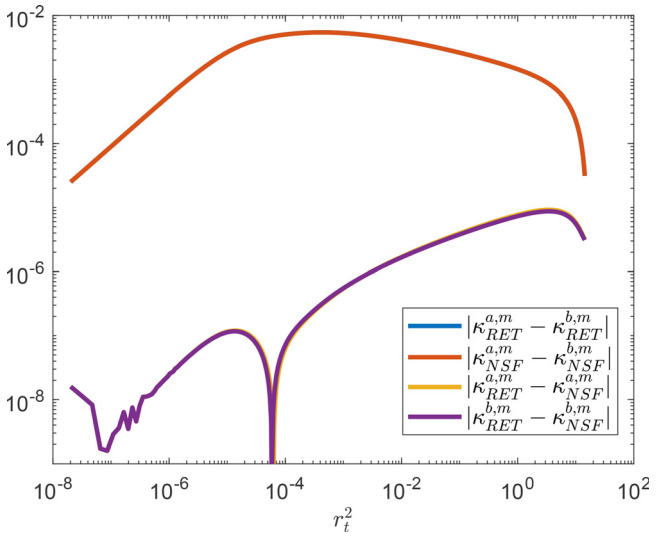

FIG. 3. A comparison of polytropic indices calculated in (43) and (46) with different models (RET and NSF, indicated as a subscript) and boundary conditions (*case a* and case *b*, indicated in the apex) as functions of r_t^2 for radon gas and $R_0 = 10^{-4}$ m.

To complete this analysis, the behavior of β_G [compared with β_L and β_{ac}, defined in (7)] is presented. Preliminarily, Fig. 5 presents the case of Argon gas for different equilibrium radii, so as to show the order of magnitude of the damping coefficients (the calculations were performed with the RET model, but NSF would have given the same results within the accuracy of the graph). Then, we focus on the effects of the molecular mass when $R_0 = 10^{-4}$ m (Fig. 6) and $R_0 = 10^{-6}$ m (Fig. 7): small radii enhance the differences between β_G terms corresponding to various monatomic gases.

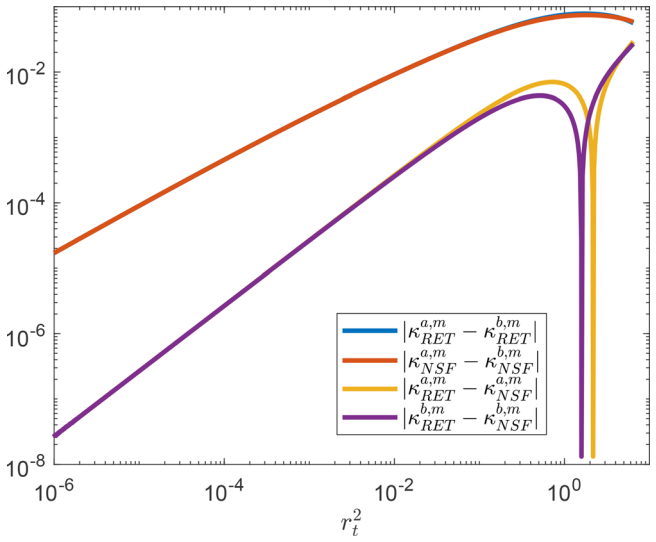

FIG. 4. A comparison of polytropic indices calculated in (43) and (46) with different models (RET and NSF, indicated as a subscript) and boundary conditions (case *a* and case *b*, indicated in the apex) as functions of r_t^2 for helium gas and $R_0 = 10^{-6}$ m.

10 January 2026 08:22:20

© Author(s) 2025

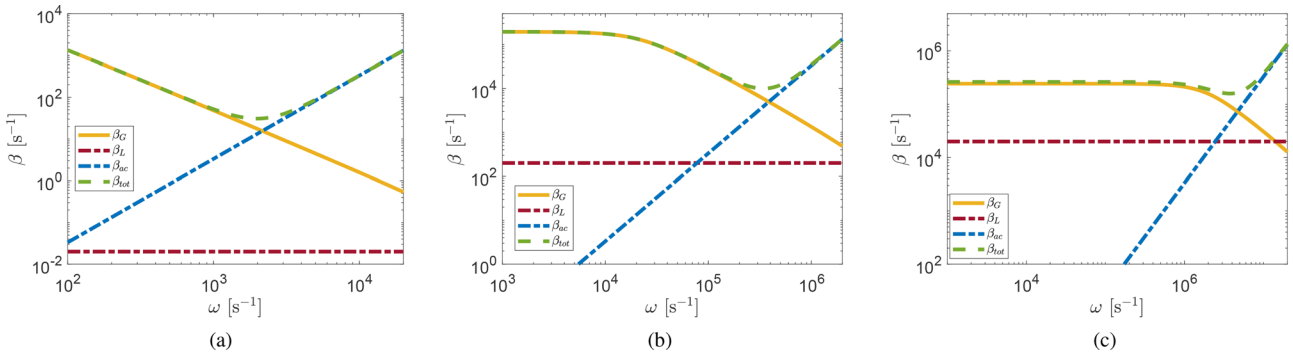

FIG. 5. A comparison between β_G determined by the RET model (boundary conditions case *a*) and all other damping coefficients introduced in (7) as functions of ω (under the homobaric condition $r_t^2 \leq 1$), when Ar gas is taken into account and $R_0 = 10^{-2}$ m (a), $R_0 = 10^{-4}$ m (b), $R_0 = 10^{-5}$ m (c).

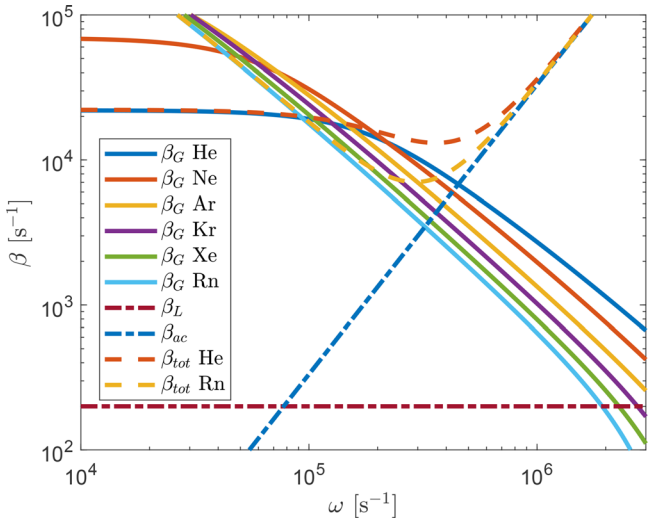

FIG. 6. The damping constant β_G derived from the RET model as a function of ω, for different monatomic gases when $R_0 = 10^{-4}$ m and *case a* is imposed.

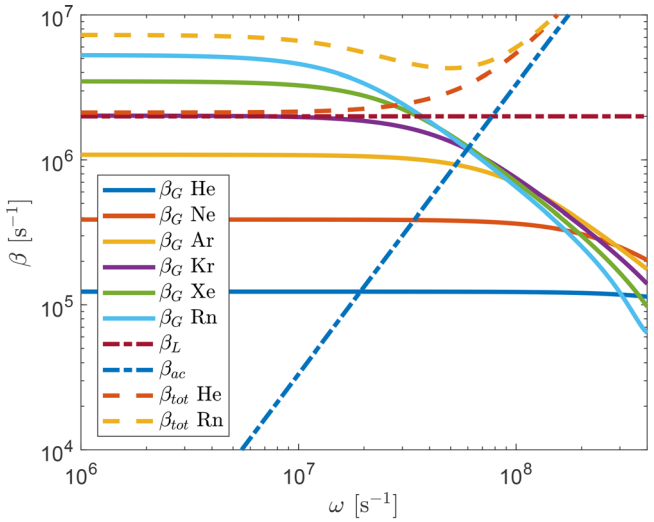

FIG. 7. The damping constant β_G derived from the RET model as a function of ω, for different monatomic gases when $R_0 = 10^{-6}$ m and *case a* is prescribed.

VI. THE ROLE OF DYNAMIC PRESSURE AND BULK VISCOSITY: THE CASE OF A POLYATOMIC GAS IN A SPHERICAL BUBBLE

In bubble dynamics, the contributions of bulk viscosity and dynamic pressure for a polyatomic gas are usually ignored. There are several reasons for this: the Stokes hypothesis (which assumes this contribution to be negligible), the fact that many gases have a very small bulk viscosity of the same magnitude order as shear viscosity, and the lack of experimental data concerning μ_b. However, in the case of CO_2 gas, very different values of the ratio between bulk and shear viscosity $r_\mu = \mu_s/\mu_b \in [1, 2000]$ are reported in the literature due to the different techniques and the different conditions in which the measurements were carried out.[46–52] To understand the potential importance of the dynamic pressure Π, one must refer to its physical interpretation. Indeed, Π is seen as the pressure difference between an equilibrium and a non-equilibrium state, but it is also related to the energy exchange between the internal and translational degrees of freedom of molecules (therefore Π refers only to polyatomic gases). The RET theory has already been successfully used to describe the effects of dynamic pressure in non-equilibrium physical conditions.[29,53–57] Moreover, we have previously shown[30,32] the role that dynamic pressure could play in both linear and nonlinear behavior of a bubble. For the sake of completeness, we briefly report those results, enriching them with different thermal conditions, an analysis of the damping coefficient, and a comparison between RET and NSF results.

The deviatoric part of the stress tensor will be neglected for the moment. Let us start from the linearization of the variables in the neighborhood of the equilibrium state $[R_E = R_0,\ \rho_E = \rho_0,\ v_E = 0,\ p_E = P_{GE} = p_0(1+w),\ q_E = 0,\ \Pi_E = 0]$, in this way, to what we obtained in (27) for a monatomic gas, we must add

$$\Pi = p_0 \Pi_1. \tag{47}$$

Under the assumptions of steady-state small amplitude oscillations, the equations of the RET model for a polytropic gas reduce to

10 January 2026 08:22:20

© Author(s) 2025

$$\rho_{G1} = i\frac{r_t^{-2}}{1+wx^2}\frac{1}{x^2}\partial_x\left(x^2V_1\right),$$
$$V_1 = i\partial_x p_{G1},$$
$$p_1 = \frac{D+2}{D} i r_t^{-2}\frac{1}{x^2}\partial_x\left(x^2V_1\right) + \frac{2}{D} i\frac{r_t^{-2}}{1+wx^2}\frac{1}{x^2}\partial_x\left(x^2Q_1\right),$$
$$\Pi_1 = i\frac{2(D-3)}{3Da_\Pi} r_r^{-2}\frac{1}{x^2}\partial_x\left(x^2V_1\right) + i\frac{4(D-3)}{3D(D+2)(1+w)a_\Pi} r_t^{-2}\frac{1}{x^2}\partial_x\left(x^2Q_1\right),$$
$$Q_1 = i\frac{(D+2)}{2}\frac{1+w}{a_q}\partial_x\left(\frac{r_t^{-2}}{x}\partial_{xx}^2(xp_{G1})\right) + i\frac{(1+w)}{2a_q}(D+2-DJ_\Pi)\partial_x p_{G1}, \tag{48}$$

where $p_{G1} = p_1 + \Pi_1$ denotes the perturbation of the total gas pressure in the bubble and a_q and a_Π are defined in (23). Moreover, referring to (25), it is easily proven that J_Π represents the ratio of Π_1 to p_{G1}, so that

$$\Pi_1 = J_\Pi p_{G1}, \quad p_1 = (1-J_\Pi)p_{G1}. \tag{49}$$

After a few mathematical steps, we obtain an equation for p_{G1} identical to (29), whose coefficients in this case turn out to be

$$a_2 = a_{2,RET}^p = 1 + a_q - \frac{D}{D+2}J_\Pi,$$
$$a_0 = a_{0,RET}^p = \frac{D}{D+2}a_q(1-J_\Pi). \tag{50}$$

It should be noted that the monatomic case analyzed in Sec. V can be easily deduced from these formulas in the limit for $D \to 3$, in which case $J_\Pi = 0$ and $\Pi = 0$. If we instead refer to the Navier–Stokes Fourier approximation, the heat flux and the dynamic pressure are described by constitutive relations involving the temperature and velocity of the gas, respectively. Hence, in system (48), the last two equations must be replaced with the following relations:

$$\Pi_1 = i\frac{2(D-3)}{3Da_\Pi^{NSF}} r_r^{-2}\frac{1}{x^2}\partial_x(x^2V_1),$$
$$Q_1 = i\frac{(D+2)}{2}\frac{1+w}{a_q^{NSF}}\left[\partial_x\left(\frac{r_t^{-2}}{x}\partial_{xx}^2(xp_{G1})\right) + \partial_x p_1\right], \tag{51}$$

where we referred to the definitions (24) and (26). After several more steps, for the perturbation of the total gas pressure in the NSF model ($\mathscr{P}_1 = p_{G1} = p_1 + \Pi_1$) we obtain an equation in the form (29), whose coefficients this time are

$$a_2 = a_{2,NSF}^p = (1+a_q^{NSF})(1-J_\Pi^{NSF}) + \frac{D}{D+2}a_q^{NSF}J_\Pi^{NSF},$$
$$a_0 = a_{0,NSF}^p = \frac{D}{D+2}a_q^{NSF}(1-J_\Pi^{NSF}). \tag{52}$$

Similarly to the case of a monatomic gas, it is possible to calculate $\lambda_j^p = \lambda_j(a_2^p, a_0^p)$, while the general form of solution (30) remains valid in this case as well.

A. Boundary conditions

In order to fix constants A_1 and A_2, we refer to the boundary conditions, already illustrated in Sec. V.

With regard to the thermal boundary conditions, we also distinguishhere between cases *a* and *b*.

Before proceeding with the calculations, it is important to make a preliminary remark. As suggested in Ref. 32, the polytropic index should be referred to as generalized, since it refers to the total gas pressure, i.e., the sum of equilibrium pressure and dynamic pressure, whereas in the literature the polytropic index usually refers only to the equilibrium pressure. For simplicity of notation, we have omitted a specific symbol for κ here, and we will do the same in the following sections (VII–X), where we will take into account other physical quantities that contribute to the determination of total gas pressure.

1. Case a

By imposing (35) and (36), it is possible to derive two relations, completely analogous to (40) if $f_{3,j}$ defined in (41) is determined as $f_{3,j} = f_{3,j}(\lambda_j^p)$ and Γ_j is replaced by Γ_j' that is defined as follows for RET or NSF models:

$$\Gamma_{j,RET}' = 1 + (\lambda_j^p)^2 - J_\Pi,$$
$$\Gamma_{j,NSF}' = 1 + (\lambda_j^p)^2 + \frac{J_\Pi^{NSF}}{1-J_\Pi^{NSF}}(\lambda_j^p)^2. \tag{53}$$

Hence, the linear algebraic system consisting of the two equations of kind (40) yields results identical to those for the monatomic case (42), provided that Γ_j is replaced with Γ_j' and $f_{3,j}$ is calculated for $\lambda_j = \lambda_j^p$. The same applies to the expressions of $\kappa^{a,p}$ and $\mu_G^{a,p}$, so for the sake of brevity, we do not report the explicit form of these coefficients, which are the same as (42) if the substitutions just described are made.

2. Case b

Taking into account the RET Eq. (48) and definitions (41) and (53), boundary conditions (35) and (39) give rise to the following algebraic system:

$$\sum_{j=1}^{2} A_j f_{3,j} = r_t^2(1+w)X_1,$$
$$\sum_{j=1}^{2} A_j\Gamma_{j,RET}' - A_L = 0,$$
$$\sum_{j=1}^{2} A_j f_{3,j}\left(\Gamma_{j,RET}' + \frac{2}{D+2}J_\Pi\right) + \Omega_L' A_L = 0, \tag{54}$$

with $\Omega_L' = i(\lambda_L+1)\frac{2a_q\omega\rho_0 T_0 k_L}{(D+2)p_0^2(1+w)^2}$. The solution of (54) is

$$A_1^{b,p} = \frac{\Gamma_2'(f_{3,2}+\Omega_L') + 2f_{3,2}J_\Pi(D+2)^{-1}}{(f_{3,1}\Gamma_2' - f_{3,2}\Gamma_1')\Omega_L' + f_{3,1}f_{3,2}(\Gamma_2' - \Gamma_1')} r_t^2(1+w)X_1,$$
$$A_2^{b,p} = -\frac{\Gamma_1'(f_{3,1}+\Omega_L') + 2f_{3,1}J_\Pi(D+2)^{-1}}{(f_{3,1}\Gamma_2' - f_{3,2}\Gamma_1')\Omega_L' + f_{3,1}f_{3,2}(\Gamma_2' - \Gamma_1')} r_t^2(1+w)X_1,$$
$$A_L^{b,p} = \frac{(\Gamma_2' f_{3,1} - \Gamma_1' f_{3,2})(1 + 2J_\Pi(D+2)^{-1})}{(f_{3,1}\Gamma_2' - f_{3,2}\Gamma_1')\Omega_L' + f_{3,1}f_{3,2}(\Gamma_2' - \Gamma_1')} r_t^2(1+w)X_1. \tag{55}$$

10 January 2026 08:22:20

© Author(s) 2025

In this case, the polytropic index and the viscosity term μ_G are derived from (22) as

$$\kappa^{b,p} = -\frac{1}{3}\Re\left(\frac{\Gamma'_2 f_{3,2} - \Gamma'_1 f_{3,1} + \Omega'_L(\Gamma'_2 - \Gamma'_1)}{(f_{3,1}\Gamma'_2 - f_{3,2}\Gamma'_1)\Omega'_L + f_{3,1}f_{3,2}(\Gamma'_2 - \Gamma'_1)} + \frac{2(f_{3,2} - f_{3,1})J_\Pi(D+2)^{-1}}{(f_{3,1}\Gamma'_2 - f_{3,2}\Gamma'_1)\Omega'_L + f_{3,1}f_{3,2}(\Gamma'_2 - \Gamma'_1)}\right) r_t^2,$$
$$\mu_G^{b,p} = -\frac{1}{4\omega}\Im\left(\frac{\Gamma'_2 f_{3,2} - \Gamma'_1 f_{3,1} + \Omega'_L(\Gamma'_2 - \Gamma'_1)}{(f_{3,1}\Gamma'_2 - f_{3,2}\Gamma'_1)\Omega'_L + f_{3,1}f_{3,2}(\Gamma'_2 - \Gamma'_1)} + \frac{2(f_{3,2} - f_{3,1})J_\Pi(D+2)^{-1}}{(f_{3,1}\Gamma'_2 - f_{3,2}\Gamma'_1)\Omega'_L + f_{3,1}f_{3,2}(\Gamma'_2 - \Gamma'_1)}\right) r_t^2 p_{GE}, \quad (56)$$

where as for coefficients $A_k^{b,p}$ e $A_L^{b,p}$, in the explicit expression of $\kappa^{b,p}$ and $\mu_G^{b,p}$, we have omitted to report the RET reference for each physical quantity.

Even in *case b*, it is possible to refer to the NSF approximation [Eqs. (48) and (51)], reducing the boundary conditions (35) and (39) to the following algebraic relations formally identical to those of the monatomic case (44), here $f_{3,j} = f_{3,j}(\lambda_j^p)$ [see (41)]:

$$\sum_{j=1}^{2} A_j f_{3,j} = r_t^2(1+w)X_1,$$
$$\sum_{j=1}^{2} A_j \Gamma'_{j,NSF} - A_L = 0, \quad (57)$$
$$\sum_{j=1}^{2} (A_j f_{3,j}\Gamma'_{j,NSF}) + \Omega'_{L,NSF}A_L = 0,$$

where in this case $\Omega'_{L,NSF} = i(\lambda_L + 1)\frac{2a_q^{NSF}\omega\rho_0 T_0 k_L}{(D+2)p_0^2(1+w)^2}$. Thus, the expression of coefficients $A_{j,NSF}^{b,p}$ and $A_{L,NSF}^{b,p}$ will be the same as in (45) if Γ_j is replaced with $\Gamma'_{j,NSF}$; the same holds also for κ and μ_G which exhibit the same structure as the corresponding quantities calculated for a monatomic gas in *case b* [see (46)]. It is possible to show that, regardless of the thermal conditions *case a* or *b*, for the polytropic index determined through the RET theory, it holds

$$\lim_{r_t \to 0} \kappa = \Re\left(\frac{1}{1 - J_\Pi}\right), \quad (58)$$

and moreover

$$\lim_{\hat{\tau}_\Pi \to 0}(1 - J_\Pi) = 1, \quad \lim_{\hat{\tau}_\Pi \to +\infty}(1 - J_\Pi) = \frac{3(D+2)}{5D}. \quad (59)$$

In other words, for high values of bulk viscosity, the limit (58) does not necessarily coincide with the isothermal value $\kappa = 1$ usually considered in the literature.

B. Some examples

Some figures are shown in order to investigate the role of the physical parameters typical of a polyatomic gas. To avoid repeating the previous remark, we do not consider the effect produced by the molecular mass of the gas, which is very similar to what can be observed in Figs. 1 and 2 for monatomic gases. The impact of bulk viscosity on κ and β_G is investigated in Figs. 8–14 for CO_2 gas (assuming[32,58] D = 7), varying the bulk viscosity through r_μ and the equilibrium radius. In what follows, as for τ_q, τ_Π will be determined from (16), assuming $p = p_{GE}$.

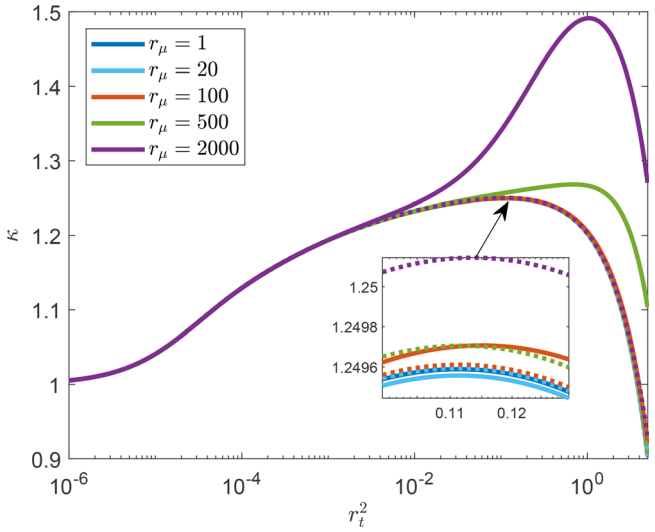

FIG. 8. A comparison between polytropic indexes determined imposing boundary conditions *case a* as functions of r_t^2 when $R_0 = 10^{-4}$ m and the ratio between the shear and the bulk viscosity is varied for CO_2 gas.

In particular, in Figs. 8 and 9, the behaviors of κ obtained by RET equations (solid line) and by NSF model (dotted line) are compared under conditions *case a*. Note that the curves corresponding to NSF coincide for any value of r_μ with the RET κ-curve drawn for $r_\mu = 1$. In other words, only the RET model could predict relevant differences on

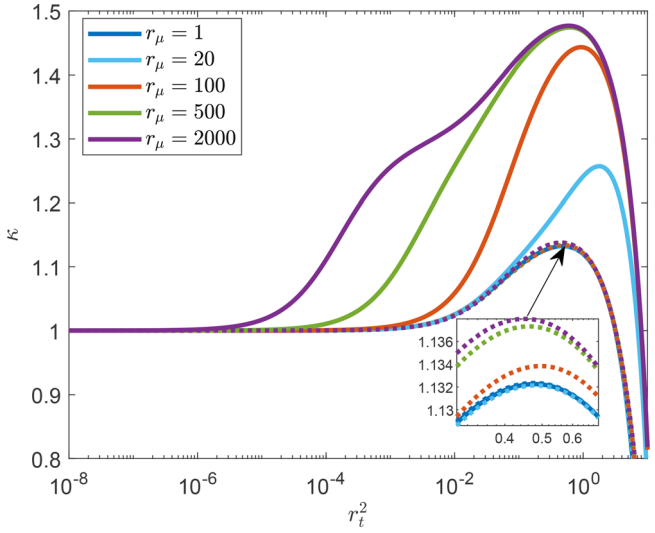

FIG. 9. A comparison between polytropic indexes determined imposing boundary conditions *case a* as functions of r_t^2 when $R_0 = 10^{-6}$ m and the ratio between the shear and the bulk viscosity is varied for CO_2 gas.

10 January 2026 08:22:20

© Author(s) 2025

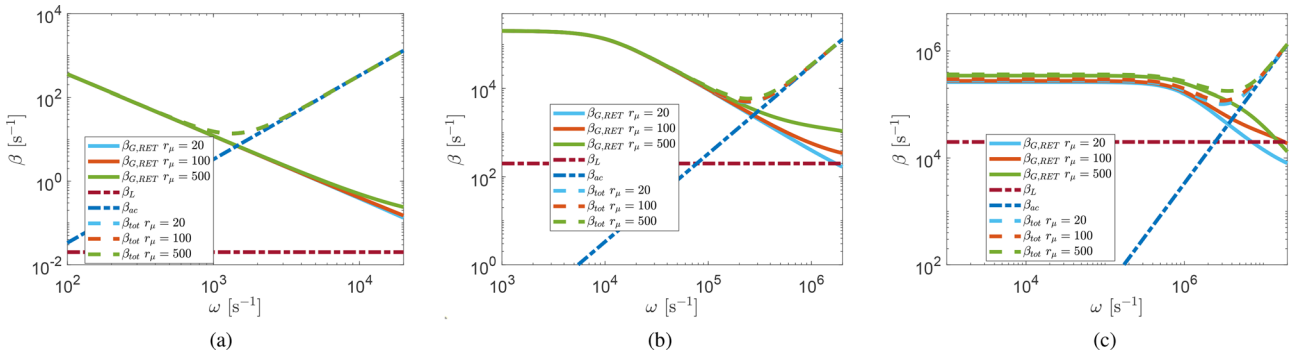

FIG. 10. A comparison between β_G determined by RET model (boundary conditions *case a* and different values of r_μ) and all other damping coefficients introduced in (7) as functions of ω (under the homobaric condition $r_t^2 \leq 1$), when CO_2 gas is taken into account and $R_0 = 10^{-2}$ m (a), $R_0 = 10^{-4}$ m (b), $R_0 = 10^{-5}$ m (c).

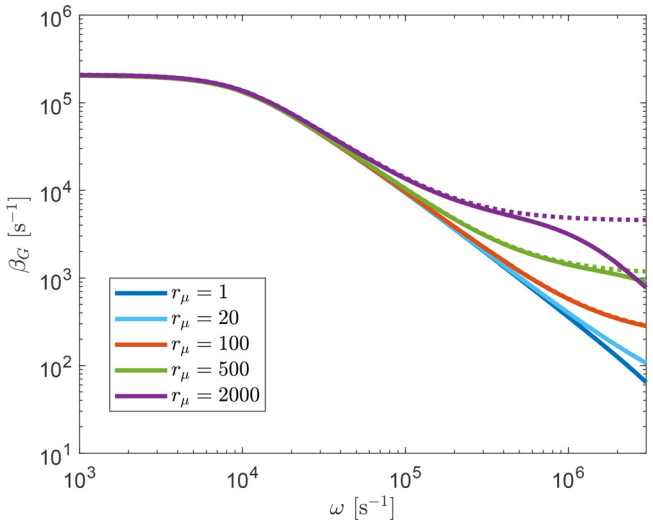

FIG. 11. A comparison between damping coefficients calculated with different models (RET in continuous line and NSF in dotted line) for boundary conditions case *a* as functions of ω when $R_0 = 10^{-4}$ m and the ratio between the shear and the bulk viscosity is varied for CO_2 gas.

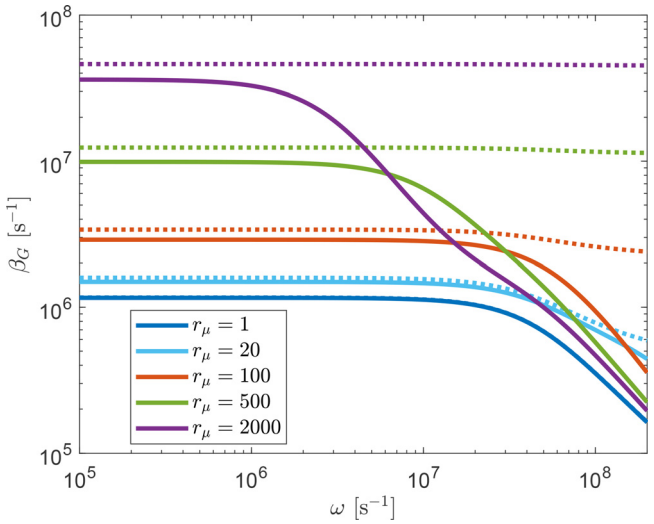

FIG. 12. A comparison between damping coefficients calculated with different models (RET in continuous line and NSF in dotted line) for boundary conditions case *a* as functions of ω, when $R_0 = 10^{-6}$ m and the ratio between the shear and the bulk viscosity is varied for CO_2 gas.

the polytropic index as the bulk viscosity increases, especially for small equilibrium radii (Fig. 9).

In Fig. 10, the damping coefficients defined in (7) for different values of r_μ are plotted as R_0 varies. In this way, it is possible to appreciate and compare the order of magnitude of β_G, β_L, and β_{ac} (the calculations were performed with the RET model): for large values of the equilibrium radius, only the thermal effects are visible, and no significant differences are observed by modifying r_μ. On the contrary, for small bubbles, β_G is mainly affected by bulk viscosity, as also confirmed by the following figures. In Fig. 11 β_G curves obtained from RET (solid line) and NSF (dotted line) coincide except for large values of ω and r_μ, when $R_0 = 10^{-4}$ m. On the contrary, in Fig. 12, for a smaller equilibrium radius ($R_0 = 10^{-6}$ m) the damping coefficient described by NSF shows a very strong μ_b dependence. Furthermore, the differences between the RET and NSF predictions become increasingly more prominent as the bulk viscosity increases (see also Figs. 13 and 14).

VII. THE ROLE OF THE GEOMETRY: SOME ROUGH MODELS OF PLANAR AND CYLINDRICAL BUBBLES

In what follows, we will consider bubbles with different shape symmetries that will be associated with the geometric parameter $N \in \{1, 2, 3\}$ already introduced in Sec. III.

We are aware that, in order to simplify the calculations and enable analytical comparisons in the small-amplitude oscillation regime, we are about to introduce oversimplified non-spherical bubble models. Nevertheless, we hope that these initial results will provide insight into the role of bubble geometry that will be developed in future works.

In particular, case $N = 1$ is represented by a gas bubble inside a thin tube filled with a liquid. We assume that the tube wall is made of a material that is neither hydrophilic nor hydrophobic, so that the contact angle between the liquid and the wall is close to 90°. In fact, it is possible to consider solids that, when properly treated, present contact

10 January 2026 08:22:20

© Author(s) 2025

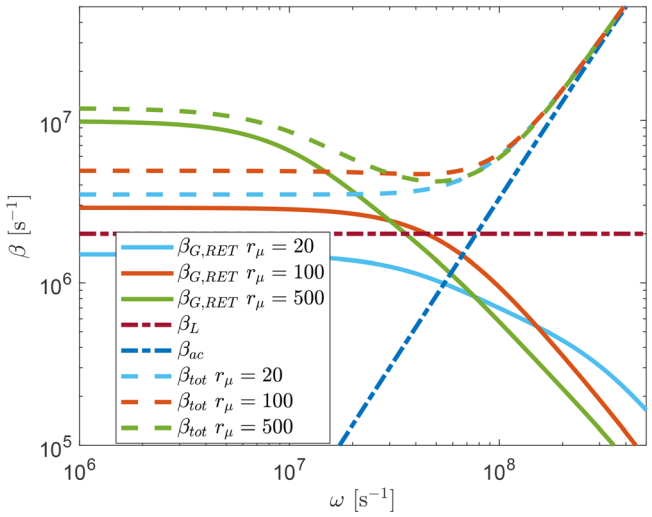

FIG. 13. A comparison between β_G determined by the RET model (boundary conditions case *a* and different values of r_μ) and all other damping coefficients introduced in (7) as functions of ω, when $R_0 = 10^{-6}$ m and CO_2 gas is taken into account.

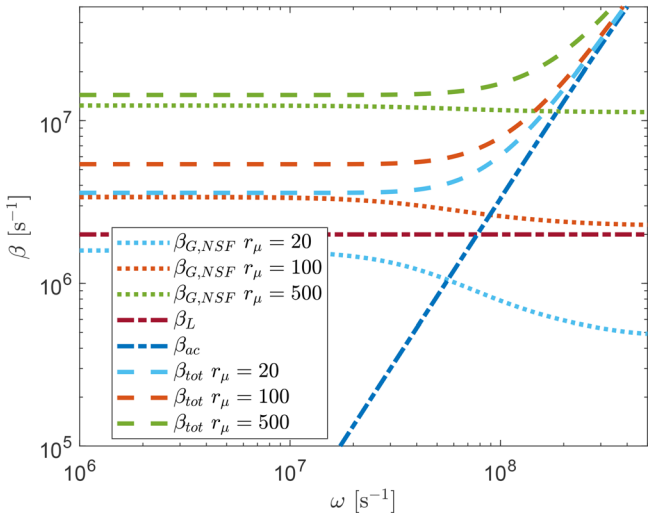

FIG. 14. A comparison between β_G determined by the NSF model (boundary conditions case *a* and different values of r_μ) and all other damping coefficients introduced in (7) as functions of ω, when $R_0 = 10^{-6}$ m and CO_2 gas is taken into account.

angles close to 90° in water (see, for example, Ref. 59). Naturally, due to the oscillation of the bubble, the contact angle could exhibit hysteresis phenomena, which are neglected here thanks to the small amplitude hypothesis. In this framework, it is reasonable to describe the bubble like a cylinder with circular cross section. If z_1 represents the coordinate along the axis of the tube, we can suppose that the bubble has its center in $z_1 = 0$ and it extends in $-H \le z_1 \le H$, while the tube goes from $-S \le z_1 \le S$. Let us also assume that the length of the bubble is significantly less than that of the tube, $2H \ll 2S$, so that edge effects can be neglected. Moreover, if the tube is rigid and thermally insulated, an adiabatic condition will apply at the lateral wall of the bubble, so the only non-zero component of gas velocity and heat flux vectors will be the one along the cylinder axis. We assume that the presence of a periodic acoustic signal applied to the liquid may induce an oscillation of the bubble along the z_1 direction, and the bubble length turns out to be a function of time $H = H(t)$, while the section of the bubble remains unchanged. A possible application of this model is represented by a gas bubble trapped in a microfluidic device[60] or in a capillary (in this case, the more complex properties linked to the nature of the tissue that constitutes the capillary are simplistically neglected). In case $N = 2$, we are instead in the presence of a cylindrical gas bubble confined in a channel, i.e., between two parallel flat plates filled with liquid. In fact, a typical experimental scenario about microfluidic devices is a shallow fluid channel between two horizontal planar walls separated by a gap thickness (for example, the channel height is fixed at 25 μm in Refs. 61 and 62). One can think, as a first approximation, that a cylindrical bubble flattened between the two walls, performs radial oscillations parallel to the two walls, excited by an external acoustic field.[62] In this case z_1 denotes the radial coordinate measured from the central axis, and we suppose that along the radial direction, the bubble extends in $z_1 \in [0, H]$, while the liquid lies around the bubble for $z_1 \in]H, S]$. Neglecting all the edge effects and assuming the presence of rigid, fixed, thermally insulated plates (or neglecting even the effects along the cylinder axis), heat flux and gas velocity vectors will only present a non-zero radial component. Cylindrical gas bubble[61,63] are relevant for several applications, in particular, we recall microfluidic devices[62] and the biomedical field.[64]

For the sake of completeness, we recall that the case $N = 3$ corresponds to the spherical geometry already extensively studied in Secs. V and VI.

A generalization of the Rayleigh–Plesset equation[13] (1) is capable of describing the behavior of $H(t)$ for different values of N, under the hypothesis of an incompressible liquid

$$\frac{1}{N-2}\left[1-\left(\frac{H}{S}\right)^{N-2}\right](H\ddot{H}+(N-1)\dot{H}^2)-\left[1-\left(\frac{H}{S}\right)^{2N-2}\right]\frac{\dot{H}^2}{2} = \frac{1}{\rho_L}\left(p_G-(N-1)\frac{\sigma_L}{H}-2(N-1)\frac{\mu_L\dot{H}}{H}-p_0+p_a\right), \tag{60}$$

where the symbols were already defined in Sec. II. We remark that for spherical geometry, S could tend to infinity, but this cannot happen for $N < 3$ given the emergence of singularities.

The equations we will use to describe the dynamics of the gas inside the bubble are those illustrated in (18) and (19), but we will now neglect the deviatoric part of the stress tensor. The calculation procedure is the same as that already illustrated in Secs. V and VI. We start from the linearization of the field variables in the neighborhood of an equilibrium configuration. Compared to what was obtained in VI, the only difference with respect to (47) is that the term of the surface tension is proportional to $N-1$, and in this way, we can rewrite the quantities w and p_{GE}, already defined in (3), as

$$w_N = (N-1)\frac{\sigma_L}{R_0}, \quad p_{GE} = p_0(1+w_N), \tag{61}$$

and express the linear expansion of the spatial quantity H and of the equilibrium pressure p consistently with the spherical case

$$H = R_0(1+X_1), \quad p = p_0(1+w_N+p_1). \tag{62}$$

10 January 2026 08:22:20

© Author(s) 2025

For notational convenience, we imagine that the equilibrium value of H is always represented by R_0 even though, at least in the 1D case, H represents a length but not a radius. As for $N = 3$, the spatial variable z_1 is replaced $x = z_1/R_0 \in [0, 1]$. Then, to go into the details of the procedure that leads to the solution of the problem, we introduce the linear operator

$$\mathscr{L}_N = \frac{1}{x^{N-1}}\partial_x(x^{N-1}\partial_x). \tag{63}$$

We remark that this operator has the same structure as the Laplacian one in the different geometries, but to avoid ambiguity in what follows, we will employ the notation (63). Under the assumption of steady-state small-amplitude oscillations, taking into account (20), (23), and (61), the system (18) with (19) reduces to an equation set of the form

$$\begin{aligned}
\rho_{G1} &= -\frac{r_t^{-2}}{(1+w_N)}\mathscr{L}_N p_{G1},\\
V_1 &= i\partial_x p_{G1},\\
p_1 = (1-J_\Pi)p_{G1} &= -\frac{D+2}{2}r_t^{-2}\mathscr{L}_N p_{G1}\\
&+\frac{2i}{D}\frac{r_t^{-2}}{1+w_N}\frac{1}{x^{N-1}}\partial_x\left(x^{N-1}Q_1\right),\\
\Pi_1 = J_\Pi p_{G1} &= -\frac{2(D-3)}{3Da_\Pi}r_t^{-2}\mathscr{L}_N p_{G1}\\
&+\frac{4i(D-3)}{3D(D+2)a_\Pi}\frac{r_t^{-2}}{1+w_N}\frac{1}{x^{N-1}}\partial_x\left(x^{N-1}Q_1\right),\\
Q_1 &= \frac{i(D+2)(1+w_N)}{2a_q}\left[\partial_x\left(r_t^{-2}\mathscr{L}_N p_{G1}+\left(1-\frac{DJ_\Pi}{D+2}\right)p_{G1}\right)\right].
\end{aligned} \tag{64}$$

After a few steps, the equation for the perturbation of the total pressure p_{G1} is obtained:

$$\mathscr{L}_N^2 p_{G1} + a^p_{2,RET} r_t^2 \mathscr{L}_N p_{G1} + a^p_{0,RET} r_t^4 p_{G1} = 0, \tag{65}$$

where the coefficients are the same as those determined in (50), and the equation for the spherical case (29) is a particular case of (67) when $N = 3$. As N varies, the solution of Eq. (67) is determined by requiring that in $x = 0$ it does not present singularities and is compatible with the condition $V_1|_{x=0} = \mathscr{Q}_1|_{x=0} = 0$. Then, it is natural to define the function

$$h_N(s,x) = \begin{cases} \dfrac{\cosh(sx)}{\cosh(s)} & \text{if } N = 1,\\ \dfrac{J_0(isx)}{J_0(is)} & \text{if } N = 2,\\ \dfrac{\sinh(sx)}{x\sinh(s)} & \text{if } N = 3, \end{cases} \tag{66}$$

where J_n denotes a Bessel function of the first kind (see the Appendix for more details), and so it is possible to write the solution in a compact way as N varies

$$p_{G1} = \sum_{j=1}^{2} A_j^N h_N(\lambda^p_{j,RET} r_t, x). \tag{67}$$

A. Boundary conditions

Determining constants A_j^N requires assigning boundary conditions. For simplicity, we will limit our analysis to the conservation of mass (35) and thermal condition *case a* (36), so that from (64), (66), and (67) it turns out that

$$\begin{aligned}
&\sum_{j=1}^{2} A_j^N f_{N,j} = r_t^2(1+w_N)X_1,\\
&\sum_{j=1}^{2} A_j^N \Gamma'_{j,RET} = 0,\\
&\text{where} \quad f_{N,j} = g_N(\lambda_j r_t), \quad \text{if}\\
&g_N(s) = \begin{cases} s\tanh(s) & \text{for } N = 1,\\ -isJ_1(is)J_0^{-1}(is) & \text{for } N = 2,\\ s\coth(s) - 1 & \text{for } N = 3. \end{cases}
\end{aligned} \tag{68}$$

The algebraic system presents a solution for A_j^N formally identical to the one obtained in the spherical case if $f_{3,j}$ is replaced by $f_{N,j}$ and the same is true for the polytropic index. By generalizing Eq. $(22)_1$ for different geometries, we easily obtain that

$$\kappa_N = -\Re\left(\frac{p_{G1}}{Np_{GE}X_1}\right). \tag{69}$$

Starting from (69) and (22), introducing the notation κ_N and $\mu_{G,N}$, where the addition of the value of N will allow us to distinguish different geometric symmetries, it must hold

$$\begin{aligned}
\kappa_N &= -\Re\left(\frac{\Gamma'_2 - \Gamma'_1}{N(\Gamma'_2 f_{N,1} - \Gamma'_1 f_{N,2})}\right)r_t^2,\\
\mu_{G,N} &= -\Im\left(\frac{\Gamma'_2 - \Gamma'_1}{4\omega(\Gamma'_2 f_{N,1} - \Gamma'_1 f_{N,2})}\right)r_t^2 p_{GE}.
\end{aligned} \tag{70}$$

To provide a first glimpse into the role of N, it is possible to analytically determine the Taylor series expansion of the polytropic index

$$\kappa_N = \Re\left(\frac{1}{1-J_\Pi} + \frac{((\lambda_1^2+\lambda_2^2)(1-J_\Pi)+\lambda_1^2\lambda_2^2)r_t^2}{c_N(1-J_\Pi)^2}\right) + O(r_t^4), \tag{71}$$
$$\text{where} \quad c_1 = 3, \quad c_2 = 8, \quad c_3 = 15.$$

Hence, the limit of κ_N for $r_t \to 0$ gives the same result as (58) and does not depend on N.

B. Some examples

The examples we report here aim to qualitatively and quantitatively study the impact of bubble geometry on the value of the polytropic index. Dotted, dashed, and continuous lines in the plot have consistently been used to distinguish $N = 1$, $N = 2$ and $N = 3$ cases, respectively. Bessel functions were calculated using the ©Matlab routine. Figures 15 and 16 consider monatomic gases with significantly different masses (He and Xe) for bubbles with $R_0 = 10^{-4}$ m (Fig. 15) and $R_0 = 10^{-6}$ m (Fig. 16). It is evident that differences due to geometry become more prominent as the bubble parameter R_0 decreases and, vice versa, they tend to disappear for large bubbles, when the geometric curvature becomes less accentuated.

10 January 2026 08:22:20

© Author(s) 2025

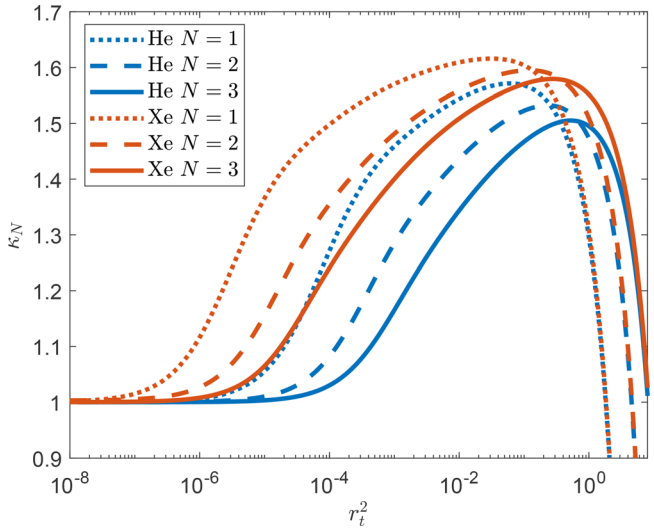

FIG. 15. The polytropic index derived from the RET model as a function of r_t^2 for different monatomic gases and different bubble geometries, when $R_0 = 10^{-4}$ m and *case a* is imposed.

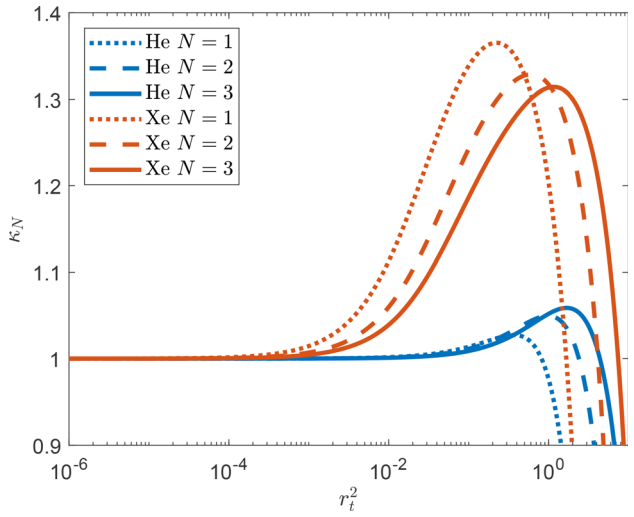

FIG. 16. The polytropic index derived from the RET model as a function of r_t^2 for different monatomic gases and different bubble geometries, when $R_0 = 10^{-6}$ m and case *a* is prescribed.

For a polyatomic gas, the effects of bulk viscosity and bubble geometry are studied together in Fig. 17 ($R_0 = 10^{-4}$ m) and Fig. 18 ($R_0 = 10^{-6}$ m). As expected, also for the CO_2 gas, the small size of the bubble enhances the role of the geometry. It should be remarked that p_{GE} varies significantly with the geometry for small values of R_0 and this naturally influences the calculation.

VIII. THE "NEGLIGIBLE" ROLE OF THE DEVIATORIC PART OF THE STRESS TENSOR

In this section, we will verify that the effect of the deviatoric part of the stress tensor is negligible, at least in the small-amplitude

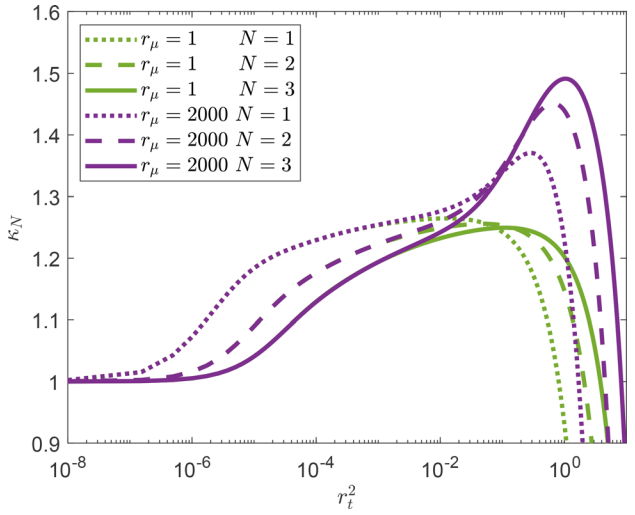

FIG. 17. The polytropic index derived from the RET model as a function of r_t^2 for a CO_2 gas with different values of r_μ and different geometries, when $R_0 = 10^{-4}$ m.

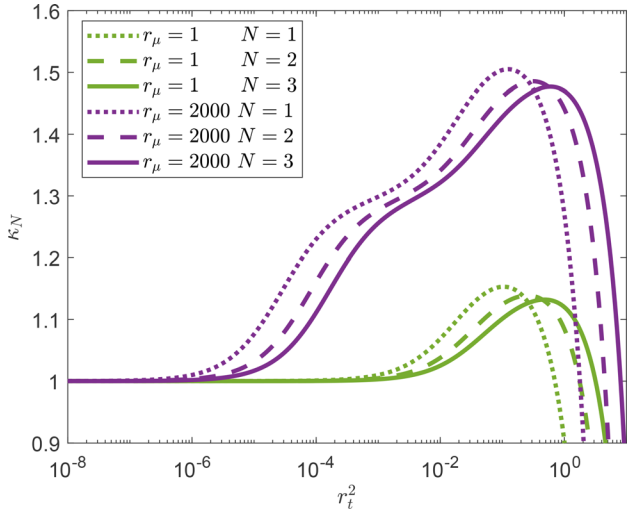

FIG. 18. The polytropic index derived from the RET model as a function of r_t^2 for a CO_2 gas with different values of r_μ and different geometries, when $R_0 = 10^{-6}$ m.

oscillation regime. This point is taken for granted in the literature[5] starting from the NSF model. To get a complete picture, we consider the different bubble geometries introduced in Sec. VII. We extend the same approach as in previous sections (V–VII) to this case, and to do so, we begin by adding the expression for the stress tensor to the linearization of the field variables described in (27) and (47)

$$\sigma^{\langle ij\rangle} = p_0 \sigma_1^{\langle ij\rangle}. \tag{72}$$

Furthermore, in order to simplify the notation of the following relations, we refer to:

$$P = p + \Pi = p_0(1 + w_N + P_1) \Rightarrow P_1 = p_1 + \Pi_1, \tag{73}$$

10 January 2026 08:22:20

© Author(s) 2025

which in this case does not represent the total gas pressure, given the presence of the deviatoric part of the stress tensor.

Referring to the quantity J_σ introduced in (25), after several steps, in the case of steady-state small amplitude oscillations, it is possible to prove that

$$\partial_x(\sigma_1^{\langle 11\rangle}) + \frac{(N-1)}{x}(\sigma_1^{\langle 11\rangle} - \sigma_1^{\langle 22\rangle}) = J_\sigma \partial_x P_1. \tag{74}$$

Thanks to this relation, system (18) with (19) is reduced to

$$\begin{aligned}
\rho_{G1} &= -\frac{r_t^{-2}}{(1+w_N)}(1-J_\sigma)\mathscr{L}_N P_1,\\
V_1 &= i(1-J_\sigma)\partial_x P_1,\\
p_1 &= i\frac{D+2}{Dx^{N-1}} r_t^{-2}\partial_x\left[x^{N-1}\left(V_1 + \frac{2Q_1}{(D+2)(1+w_N)}\right)\right],\\
\Pi_1 &= i\frac{2(D-3)}{3Da_\Pi x^{N-1}} r_t^{-2}\partial_x\left[x^{N-1}\left(V_1 + \frac{2Q_1}{(D+2)(1+w_N)}\right)\right],\\
\sigma_1^{\langle 11\rangle} &= -i\frac{4x^{(N-1)/2}}{3a_\sigma} r_t^{-2}\partial_x\left[\frac{1}{x^{(N-1)/2}}\left(V_1 + \frac{2Q_1}{(D+2)(1+w_N)}\right)\right],\\
\sigma_1^{\langle 22\rangle} &= i\frac{2x^{\ell(N)/2}}{3a_\sigma} r_t^{-2}\partial_x\left[\frac{1}{x^{\ell(N)/2}}\left(V_1 + \frac{2Q_1}{(D+2)(1+w_N)}\right)\right],\\
Q_1 &= i\frac{D+2}{2}\frac{1+w_N}{a_q}\partial_x\left[r_t^{-2}(1-J_\sigma)\mathscr{L}_N P_1\right.\\
&\quad \left. + \left(1 - \frac{D}{D+2}J_\Pi - \frac{2}{D+2}J_\sigma\right)P_1\right],
\end{aligned} \tag{75}$$

where

$$\ell(N) = (N-1)(10-3N). \tag{76}$$

Regarding this last quantity, the key to obtaining identity (74) lies in the fact that for $N \in \{1,2,3\}$ (i.e., the cases of interest in this analysis) the following holds: $(N-1)(2-N-\ell(N)/2) = -2(N-1)$.

From (75), we deduce that the equation for P_1 takes the usual form of (67), albeit with modified coefficients. These coefficients are denoted here by the letter b to distinguish them from those obtained in other sections of this work, where we will never take into account the presence of $\sigma^{\langle ij\rangle}$

$$\begin{aligned}
&\mathscr{L}_N^2 P_1 + b_2 r_t^2 \mathscr{L}_N P_1 + b_0 r_t^4 P_1 = 0,\\
&b_2 = 1 + a_q + \frac{D}{D+2}\frac{J_\sigma - J_\Pi}{1-J_\sigma}, \quad b_0 = \frac{D}{D+2}\frac{1-J_\Pi}{1-J_\sigma}a_q.
\end{aligned} \tag{77}$$

This equation is associated with a characteristic polynomial of the same form as (31) and it is important to stress that the roots of the polynomial are given by $\lambda_j = \lambda_j(b_2, b_0)$ with $j = 1, 2$, if λ_j indicates the function expressed in (32). Therefore, the general solution of (77) has the same structure described in Sec. VII

$$P_1 = \sum_{j=1}^{2} B_j^N h_N(\lambda_j r_t, x), \tag{78}$$

where the coefficients of the linear combination of the possible solutions are denoted by B_j^N (and not A_j^N) in order to highlight the presence of $\sigma^{\langle ij\rangle}$ here as well.

A. Boundary conditions

As usual, to fix the values of the coefficients in (78), it is necessary to introduce appropriate boundary conditions at the interface between the gas and the liquid. For the sake of simplicity, we will limit ourselves to mass conservation (35) and *case a* (36), so as to obtain two algebraic equations in the two unknowns B_1 and B_2

$$\begin{aligned}
&\sum_{j=1}^{2} B_j^N f_{N,j} = \frac{r_t^2(1+w_N)X_1}{1-J_\sigma},\\
&\sum_{j=1}^{2} B_j^N \Gamma_j'' = 0,\\
&\text{with} \quad \Gamma_j'' = 1 + \lambda_j^2 - J_\Pi - J_\sigma\lambda_j^2.
\end{aligned} \tag{79}$$

The structure of the equations remains the same as in the previous cases, and, therefore, the solution also takes the same form as (42) except for the presence of the factor $(1-J_\sigma)^{-1}$

$$\begin{aligned}
B_1^N &= \frac{1}{1-J_\sigma}\frac{\Gamma_2'' r_t^2(1+w_N)X_1}{\Gamma_2'' f_{N,1} - \Gamma_1'' f_{N,2}},\\
B_2^N &= -\frac{1}{1-J_\sigma}\frac{\Gamma_1'' r_t^2(1+w_N)X_1}{\Gamma_2'' f_{N,1} - \Gamma_1'' f_{N,2}}.
\end{aligned} \tag{80}$$

To determine the polytropic index, however, we must refer to the perturbation of the total gas pressure at the bubble wall

$$p_{G1}|_b = (P_1 - \sigma_1^{\langle 11\rangle})|_b, \quad \text{with } P_1|_b = B_1^N + B_2^N, \tag{81}$$

furthermore, if we indicate with S_j^N the quantity

$$\begin{aligned}
S_j^N = &\frac{2}{3a_q a_\sigma}\left[(1-J_\sigma)(1+a_q+\lambda_j^2) + \frac{D}{D+2}(J_\sigma - J_\Pi)\right]\\
&\times\left(2\lambda_j^2 - 3(N-1)f_{N,j}r_t^{-2}\right),
\end{aligned} \tag{82}$$

it must hold

$$\sigma_1^{\langle 11\rangle}|_b = \sum_{j=1}^{2} B_j^N S_j^N. \tag{83}$$

Finally, referring to (69) and $(22)_2$, the polytropic index and the viscosity term μ_G in the presence of the deviatoric part of the stress tensor and for $N = 1, 2, 3$ turn out to be

$$\begin{aligned}
\kappa_{N,\sigma} &= -\Re\left[\frac{r_t^2}{N(1-J_\sigma)}\frac{\Gamma_2''(1-S_1^N) - \Gamma_1''(1-S_2^N)}{\Gamma_2'' f_{N,1} - \Gamma_1'' f_{N,2}}\right],\\
\mu_{G,N,\sigma} &= -\Im\left[\frac{r_t^2 p_0(1+w_N)}{4\omega(1-J_\sigma)}\frac{\Gamma_2''(1-S_1^N) - \Gamma_1''(1-S_2^N)}{\Gamma_2'' f_{N,1} - \Gamma_1'' f_{N,2}}\right].
\end{aligned} \tag{84}$$

B. Some examples

In what follows, as done for the other relaxation times, τ_σ will be determined by referring to (16) and assuming $p = p_{GE}$.

Figures 19 and 20 provide a comparison between the model that takes into account the deviatoric part of the stress tensor and the one that neglects it (already illustrated in Figs. 15 and 16, respectively). It is evident that in spherical symmetry, even for very small radii and very

10 January 2026 08:22:20

© Author(s) 2025

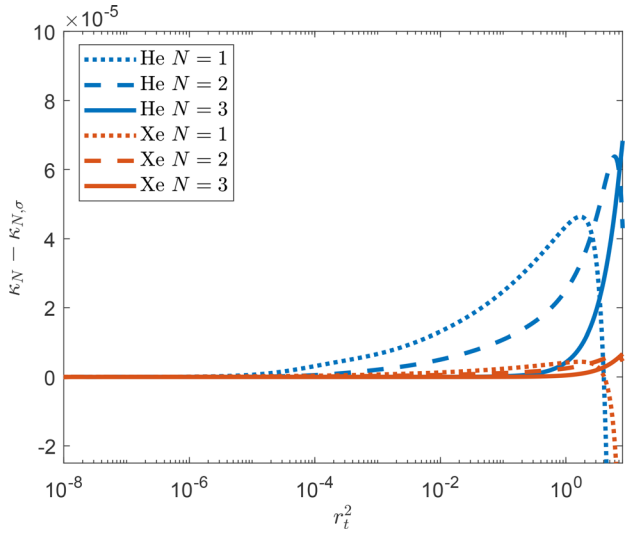

FIG. 19. The differences between the polytropic index derived from the RET model without and with the deviatoric part of the stress tensor (denoted by κ_N and $\kappa_{N,\sigma}$, respectively) as a function of r_t^2 for different monatomic gases and different bubble geometries, when $R_0 = 10^{-4}$ m and case *a* is imposed.

small molecular masses of the gas, the effect of $\sigma^{\langle ij\rangle}$ can be deemed completely negligible. This is not true for $N = 1$, when the bubble size is very small and helium gas is being considered. However, it should be recalled that the latter is an extreme case, rather of mathematical than of physical interest, and it can be concluded that generally the stress tensor affects κ very modestly and therefore can be reasonably neglected.

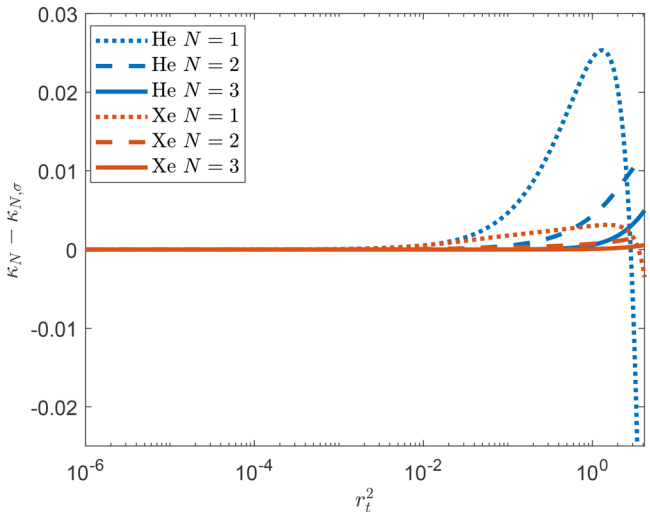

FIG. 20. The differences between the polytropic index derived from the RET model without and with the deviatoric part of the stress tensor (denoted by κ_N and $\kappa_{N,\sigma}$, respectively) as a function of r_t^2 for different monatomic gases and different bubble geometries, when $R_0 = 10^{-6}$ m and *case a* is imposed.

IX. THE ROLE OF THE HOMOBARIC ASSUMPTION

A. The model construction

In this section, as previously announced, we once again ignore the deviatoric terms of the stress tensor. We have already mentioned the importance of the homobaric assumption in ensuring stability in the bubble. However, we have not specified that this assumption is also the key, first used by Prosperetti,[5,37] for constructing a simplified model of the gas in the bubble—a homobaric model, precisely. Following Prosperetti's idea, we have already introduced[32] a homobaric model that takes into account the dynamic pressure in a spherically symmetric bubble. Here, we also deduce the equations for the planar and cylindrical cases, before moving on to a comparison of κ and β_G in the regime of small-amplitude oscillations. We start from Eqs. (14) and (15), we neglect $\sigma^{\langle ij\rangle}$ and we integrate $(14)_3$ and $(15)_1$ in a volume with the form of

- a cylinder that presents the same fixed section of the tube containing the bubble and $z_1 \in [-r, r]$ if $r \leq H(t)$ (for the case $N = 1$);
- a cylinder of given height and circular cross-section of radius $z_1 = r \leq H(t)$ in the case $N = 2$;
- a sphere centered in the center of the bubble with radius $z_1 = r \leq H(t)$ [where to make the notation homogeneous in the three cases we have indicated $R(t)$ with the symbol $H(t)$] when $N = 3$.

Having introduced the homobaricity assumption, i.e., that both p and Π are homogeneous quantities in space (this hypothesis is reasonable for Π at least in the regime of small-amplitude oscillations, see Sec. VI and Ref. 32) and exploiting the divergence theorem, we obtain an equation for the velocity component along z_1, v_1, which also involves the heat flux component along z_1, q_1

$$v_1 = -\frac{2}{(D+2)p + 2\Pi}\left[\frac{Dz_1}{2N}\dot{p} + q_1\right]. \tag{85}$$

We also obtain the following equations, considering the limit for $r \to H(t)$ and imposing the mass conservation condition inside the bubble, i.e., $v_1|_b = \dot{H}$

$$\dot{p} = -\frac{2N}{DH}\left[\frac{(D+2)p + 2\Pi}{2}\dot{H} + q_1|_b\right],$$
$$\dot{\Pi} = -N\left(\frac{2(D-3)(p+\Pi)}{3D} + \Pi\right)\frac{\dot{H}}{H} - \frac{4N(D-3)}{3D(D+2)H}q_1|_b - \frac{\Pi}{\tau_\Pi}. \tag{86}$$

The variable $y = r/H(t) \in [0, 1]$ is commonly introduced, so that (85) can be rewritten as

$$v_1 = \dot{H}y + 2\frac{q_1|_b y - q_1}{(D+2)p + 2\Pi}. \tag{87}$$

These equations replace the $(18)_{2,4,5}$. Then, $(18)_{3,7}$ are neglected since, as already mentioned, $\sigma^{\langle ij\rangle}$ are assumed to be negligible. Furthermore, the mass conservation equation $(18)_1$ is replaced by the following integral condition, exploiting the ideal gas hypothesis

$$M_0 = \iiint_{\mathscr{B}_N} \rho dV = \frac{pm}{k_B}\iiint_{\mathscr{B}_N}\frac{1}{T}dV, \tag{88}$$

10 January 2026 08:22:20

© Author(s) 2025

where M_0 represents the total mass of the gas contained in the bubble and $\mathscr{B}_N$ indicates the bubble in the three geometries described by the parameter N. In a few steps, the previous condition is reduced to

$$p = \frac{p_0(1+w_N)R_0^N}{NH(t)^N I_N} \quad \text{if} \quad I_N = \int_0^1 x^{N-1}(T/T_0)^{-1}dx. \tag{89}$$

Finally, referring to y and starting from the previous relations and $(18)_{5,6}$, it is possible to deduce the equations for temperature and heat flux in the following form:

$$\begin{aligned} &\frac{\Delta}{2T}\left[\partial_t T + \frac{v-\dot{H}y}{H}\partial_y T\right] + \frac{1}{Hy^{N-1}}\partial_y(y^{N-1}q) - \frac{p+\Pi}{p}\dot{p} = 0,\\ &\partial_t q + \frac{p\Delta}{2\rho T H}\partial_y T = -\frac{q}{\tau_q} - \frac{q\dot{H}}{H(D+2)}[(N+1)(D+4)+2], \end{aligned} \tag{90}$$

if $\Delta = (D+2)p + 2\Pi$.

B. The small amplitude oscillation regime

Under the assumption of steady-state small amplitude oscillations the previous equations are linearized, after having replaced y with its linearized analogue $x = z_1/R_0$

$$\begin{aligned} p_1 &= -N\frac{D+2}{D}(1+w_N)X_1 + i\frac{2Nr_t^{-2}}{D(1+w_N)}Q_1|_b\\ \Pi_1 &= -\frac{2N(D-3)}{3Da_\Pi}(1+w_N)X_1 + i\frac{4N(D-3)}{3D(D+2)a_\Pi}\frac{r_t^{-2}}{1+w_N}Q_1|_b,\\ T_1 &= \frac{2p_1}{(D+2)(1+w_N)} + i\frac{2r_t^{-2}}{(D+2)(1+w_N)^2}\frac{\partial_x(x^{N-1}Q_1)}{x^{N-1}}\\ Q_1 &= i\frac{(D+2)(1+w_N)^2}{2a_q}\partial_x T_1, \end{aligned} \tag{91}$$

from which the equation for T_1 turns ou to be

$$\mathscr{L}_N T_1 + c_0 r_t^2 T_1 = c_0 c_c r_t^2 p_1, \quad c_0 = a_q, \quad c_c = \frac{2}{(D+2)(1+w_N)}. \tag{92}$$

Note that, as in Sec. VI, it is easily verified that $\Pi_1 = J_\Pi(p_1+\Pi_1)$. If we denote $\lambda' = \sqrt{-c_0}$, the general solution of (92) can be expressed referring to (66) as

$$T_1 = c_c p_1 + C_N h_N(\lambda' r_t, x), \tag{93}$$

where solutions that present singularities at $x = 0$ or for which the velocity and heat flux do not vanish at $x = 0$ have accordingly been discarded.

C. Boundary conditions

To determine the constant C_N, a boundary condition must be assigned. This point seems to be at odds with the cases analyzed in Secs. V–VIII, in which at least two conditions were always imposed. It should be noted, however, that the mass conservation condition has already been imposed to derive the model and is therefore implicitly valid in all cases. For simplicity, we will limit here to the consideration of *case a* (36). Taking into account Eq. $(91)_{1,4}$ and introducing the quantities f_N defined on the basis of (68)

$$f_N = g_N(\lambda' r_t). \tag{94}$$

It is easily proven that

$$p_1 = -\frac{N(D+2)(1+w_N)X_1}{D + 2N(\lambda' r_t)^{-2} f_N}, \tag{95}$$

and, therefore, from (22) and (69) it holds

$$\begin{aligned} \kappa_{N,h} &= -\Re\left(\frac{p_1+\Pi_1}{N(1+w_N)X_1}\right)\\ &= \Re\left[\frac{(D+2)}{(1-J_\Pi)(D+2N(\lambda' r_t)^{-2}f_N)}\right],\\ \mu_{G,N,h} &= \Im\left[\frac{N(D+2)p_0(1+w_N)}{4\omega(1-J_\Pi)(D+2N(\lambda' r_t)^{-2}f_N)}\right]. \end{aligned} \tag{96}$$

Before moving on to a numerical comparison between the polytropic index determined through the homobaric model $\kappa_{N,h}$ and the one obtained in Sec. VII κ_N, it is convenient to analytically determine isothermal and adiabatic limits

$$\lim_{r_t\to 0}\kappa_{N,h} = \Re\left[\frac{1}{1-J_\Pi}\right], \quad \lim_{r_t\to+\infty}\kappa_{N,h} = \frac{D+2}{D}\Re\left[\frac{1}{1-J_\Pi}\right], \tag{97}$$

where (59) holds as well. Thus, the homobaric model overcomes the problem of the nonexistence of the adiabatic limit of κ. However, this limit must be treated with caution since we are entering the non-homobaric region where the model itself loses its meaning and validity.

D. Some examples

The following figures are meant to show the behavior of the polytropic index and damping coefficient derived from the homobaric model in order to highlight the role of the homobaricity assumption. In Fig. 21, the same parameters as in Fig. 16 are prescribed to make such a comparison possible. However, we stress that we have omitted the plot of the oscillations of κ in the non-homobaric regime case as r_t increases, in order to avoid the graphs being incomprehensible. Strictly speaking, the homobaric hypothesis is valid as long as the graphs of $\kappa_{N,h}$ and κ_N coincide or differ slightly. However, in practice, the validity of the homobaric hypothesis is sometimes extended to the case in which κ_N is positive, that is, when the stability of the bubble is guaranteed. Let r_t^* denote the value for which $\kappa_{N,h}$ and κ_N differ significantly when $r_t > r_T^*$. From Fig. 21, it is evident that r_t^* is influenced by geometry (it is smaller for $N = 1$) and gas properties. As a general rule, it can be said that $r_t^* \lesssim 1$.

Figure 22 presents the behavior of the damping coefficient β_G [determined from (7) and (96)] for two different monatomic gases, different geometries, and homobaric and non-homobaric models (the parameters are prescribed as in the previous figure). In this regard, a less significant difference is observed in the transition from non-homobaric to homobaric models, especially with $N = 1$, to the point that the two dotted lines for helium gas are practically indistinguishable. For xenon, the differences become evident only for high values of ω.

10 January 2026 08:22:20

© Author(s) 2025

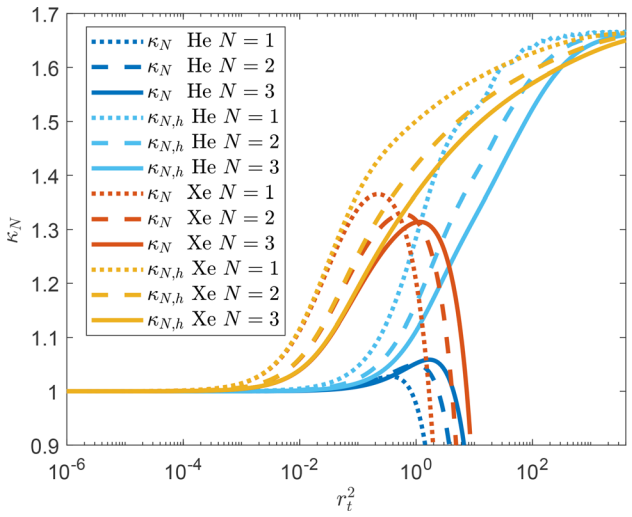

FIG. 21. A comparison between polytropic indexes derived from the model with and without the homobaric assumption [denoted by κ_N in (69) and $\kappa_{N,h}$ in (96), respectively] as a function of r_t^2 [defined in (20)] for different monatomic gases and different bubble geometries, when $R_0 = 10^{-6}$ m.

X. THE ROLE OF MASS TRANSFER

Up to now, we have always considered cases where the mass of the gas inside the bubble is conserved. In this section, instead we will attempt to investigate the consequences of mass transfer. To remain within the scope of gas bubble analysis, we will neglect vapor effects, and for this purpose, we will set the liquid temperature far from its boiling point. We recall that the case of vapor bubbles, even for small-amplitude oscillations, has been extensively studied in the literature[65]

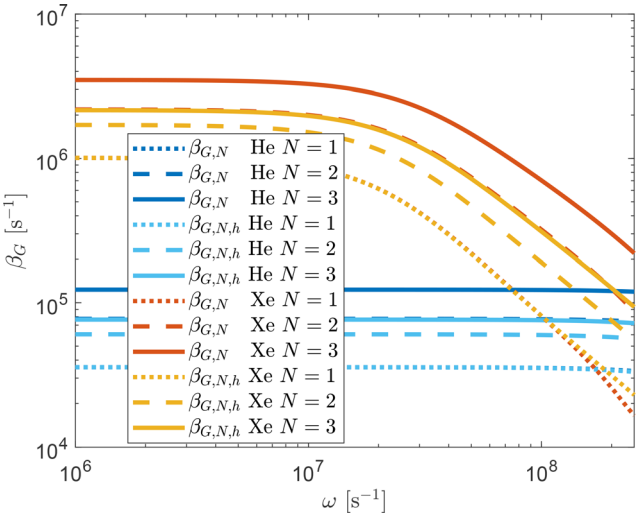

FIG. 22. A comparison between damping coefficients β_G derived from models without and with the homobaric assumption (denoted by $\beta_{G,N}$ and $\beta_{G,N,h}$, respectively) as a function of the angular frequency ω for different monatomic gases and different bubble geometries, when $R_0 = 10^{-6}$ m. In particular $\beta_{G,N}$ and $\beta_{G,N,h}$ are calculated from (7), referring to $\mu_{G,N}$ in (70) and $\mu_{G,N,h}$ in (96).

(for aspects of linear behavior, see, for example, Ref. 66). To include phase change in the present framework, one could refer to the pioneering work by Fujikawa and Akamatsu and more recent developments,[16,67] integrating into the mathematical model two thermodynamic boundary layers at the gas–liquid interface and considering the energy balance both within the bubble and in the surrounding liquid.

It must be stressed that only spherical bubbles will be studied here.

A. Gas diffusion

In the case of gas diffusion, an expansion of the equations in the neighborhood of an equilibrium state requires special, unlikely conditions regarding the density of the gas dissolved in the liquid ρ_g. As a matter of fact, it is not sufficient to assume a generic condition of oversaturation of the liquid to guarantee bubble equilibrium in the absence of an acoustic forcing. Henry's law at equilibrium must hold in the form

$$\rho_g = \rho_{g0} = \frac{S}{H(T_0)} p_{GE}, \tag{98}$$

where $S = \rho_L m_G / m_L$, if m_L denotes the liquid molecular mass, while m_G is one of the gases, and $H(T)$ represents the well-known Henry's constant, which depends on the gas and liquid involved and is determined experimentally as a function of temperature. In the absence of acoustic driving pressure, any initial value of ρ_g that does not satisfy (98) gives rise to a situation of imbalance. As a matter of fact, for $\rho_g < \rho_{g0}$, the bubble's volume progressively decreases until it dissolves due to gas diffusion from the bubble into the liquid. On the contrary, when $\rho_g > \rho_{g0}$, gas diffuses from the surrounding layer into the bubble, causing it to expand.

The oversimplified study we will present here is not intended to represent a general case, but rather to describe the linear effects of a phenomenon that remains purely nonlinear and is observable over long timescales. Rectified diffusion, that is to say, the progressive growth of the bubble's average radius due to gas diffusion phenomena, is numerically and experimentally significant only after a large number of oscillation cycles and under highly nonlinear conditions.[7]

Given these premises, let us imagine to insert a small amplitude acoustic forcing and focus on the linear oscillation regime described in Sec. VI for a spherical bubble containing a polyatomic ($D > 3$) or monatomic ($D = 3$) gas described by RET. The behavior of gas pressure inside the bubble is given by (30). To determine the constant coefficients A_j, it is necessary to impose boundary conditions at the bubble wall. Starting with the gas-liquid diffusion equation for ρ_g we can write

$$\partial_t \rho_g + \frac{R^2}{r^2} \dot{R} \partial_r \rho_g = D_L \nabla^2 \rho_g, \tag{99}$$

where r represents the radial variable $r \in]R, \infty]$ in the region around the bubble occupied by the liquid. The velocity of the liquid has been determined under the assumption of incompressibility as $(R/r)^2 \dot{R}$ and D_L indicates the mass diffusivity of the gas in the liquid. The condition associated with the previous equation is

$$\lim_{r \to \infty} \rho_g = \rho_{g0}. \tag{100}$$

10 January 2026 08:22:20

© Author(s) 2025

Under the assumption of small amplitude steady-state oscillations, referring to $x = r/R_0 \in]1, \infty]$, we linearize both the variable ρ_g and Eq. (99)

$$\rho_g = \rho_{g0}(1 + \rho_{g1}), \quad i\frac{\omega R_0^2}{D_L}\rho_{g1} = \frac{1}{x^2}\partial_x(x^2\partial_x\rho_{g1}). \tag{101}$$

We stress that for passive dissolution of the bubble,[68] the convective term in (99) is commonly eliminated, thus decoupling the equation for ρ_g from the equation for the bubble radius. However, it is well-known that such a term cannot be neglected in the case of rectified diffusion (i.e., in the presence of the acoustic forcing) without compromising the correctness of the results.[7,69] The present analysis cannot include nonlinear terms, and, indeed, shows that in a linear regime it is reasonable to ignore gas diffusion. However, taking into account (100) for the general solution of the previous equation, it must hold that $\lim_{x\to\infty}\rho_{g1} = 0$, that is to say,

$$\rho_{g1} = C_1\frac{\exp[-\lambda_D(x-1)]}{x}, \quad \text{if } \lambda_D = i^{1/2}R_0\sqrt{\omega D_L^{-1}}. \tag{102}$$

Applying Henry's law

$$\rho_g|_b = \frac{S}{H(T)}p|_b, \tag{103}$$

(98) and the first-order expansion imply that

$$\rho_{g1}|_b = \rho_{g1}(x=1,t) = \frac{S}{H(T_0)}\frac{p_0 p_1|_b}{\rho_{g0}}, \tag{104}$$

and it turns out that

$$C_1 = \frac{(1-J_\Pi)}{1+w}(A_1 + A_2). \tag{105}$$

The coefficients A_j remain to be determined using temperature and velocity conditions for the gas at the bubble wall. Regarding the velocity, one can write

$$[\rho(\dot{R} - v)]|_b = D_L\partial_r\rho_g|_b, \tag{106}$$

where for the quantities ρ and v, relative to the gas in the bubble, linearization (47) and Eq. (48) hold. Thus, it is possible to obtain the relation

$$\sum_{j=1}^{2} A_j f_{3,j} = r_t^2(1+w)X_1 - i\Delta_D(A_1 + A_2), \tag{107}$$

if $\Delta_D = \omega D_L S(1-J_\Pi)(i^{1/2}\lambda_D + 1)/H(T_0)$. Finally, we impose the thermal condition, referring to *case a* (35), already illustrated in Secs. V and VI. Starting from (22), (53), and (107) it holds

$$\begin{aligned}\kappa_D &= -\Re\left(\frac{\Gamma_2' - \Gamma_1'}{3(f_{3,1}\Gamma_2' - f_{3,2}\Gamma_1' + i\Delta_D(\Gamma_2' - \Gamma_1'))}\right)r_t^2,\\ \mu_{G,D} &= -\Im\left(\frac{(\Gamma_2' - \Gamma_1')p_{GE}}{4\omega(f_{3,1}\Gamma_2' - f_{3,2}\Gamma_1' + i\Delta_D(\Gamma_2' - \Gamma_1'))}\right)r_t^2.\end{aligned} \tag{108}$$

Note that in the absence of gas diffusion, the limit $D_L \to 0$ holds, Δ_D vanishes as well, and relations (108) coincide with the corresponding ones for a polyatomic gas under the assumption of mass conservation.

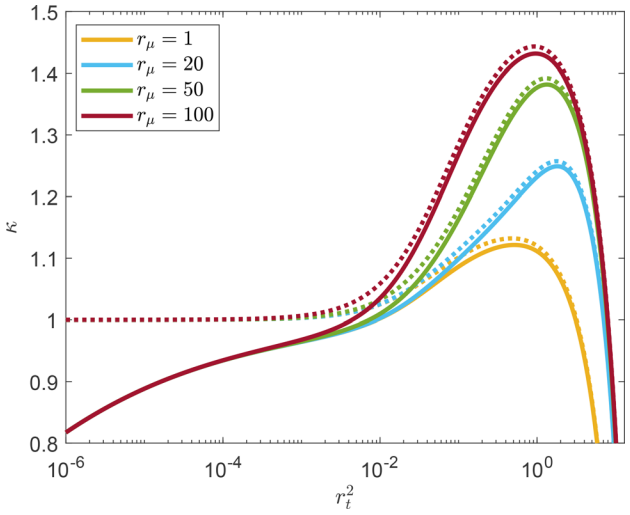

FIG. 23. The polytropic index derived from the RET model in the diffusive *case* (plotted in continuous line) and under the assumption of mass conservation (plotted in dotted line), as a function of the dimensionless parameter r_t^2, for CO_2 gas with different values of r_μ, when $R_0 = 10^{-6}$ m.

For the sake of completeness, in Fig. 23, we compare the behavior of κ in the presence of gas diffusion [formula (108)—continuous line] and in the case of mass conservation [as determined in Sec. VI in *case a*—dotted line], we refer to CO_2 gas, when $R_0 = 10^{-6}$ m and different values of r_μ are prescribed. For small values of r_t, i.e., when ω is small, there is no coincidence between continuous and dotted curves, and in the case of mass transfer, κ drops below 1. On the contrary, an overlap between continuous and dotted curves appears as ω increases.

XI. THE ROLE OF A SHELL

In the past few decades, coated micro-bubbles have gained increasing importance in medicine. In particular, ultrasound contrast agents (UCA) are gas bubbles enclosed in a shell made of a thin layer, often a lipid monolayer,[17,19] that are currently used to enhance ultrasound imaging for blood flow or tissues. For the sake of completeness, we recall that bubbles confined in shells are also employed to deliver drugs or therapeutic agents,[17,19] but in this section, we will focus on UCAs.

Equations for the evolution of the radius of a coated gas bubble, assumed to be spherical, are deduced from (2) by replacing p_L with the expression p_{uca}, which takes into account shell effects. In particular, in the case of a lipid monolayer, a viscous pressure term is introduced. This is commonly derived from Newton's linear viscous law for a shell of infinitesimal thickness and is proportional to the surface dilatation viscosity of the monolayer, denoted by k_s.[70–73]

$$p_{vis} = 4k_s\dot{R}R^{-2}. \tag{109}$$

The surface tension term $2\sigma_S/R$ must also be appropriately modified to take into account the presence of the shell, and numerous models are available in the literature to describe σ_S. Here, we refer to the one introduced by Marmottant *et al.*,[72] which provides

10 January 2026 08:22:20

© Author(s) 2025

$$\sigma_S = \begin{cases} 0 & \text{if } R \le R_b, \\ \chi\left(\dfrac{R^2}{R_b^2} - 1\right) & \text{if } R_b \le R \le R_r, \\ \sigma_L & \text{if } R \ge R_r. \end{cases} \tag{110}$$

The idea introduced by this formula is that the behavior of σ_S is strongly dependent on the bubble radius. In particular, due to the buckling phenomenon, the surface tension vanishes if the bubble presents a radius smaller than the critical value R_b. However, as the radius increases, the value of σ_S increases until the monolayer breaks, i.e., R reaches R_r. If the bubble radius exceeds the rupture radius, the surface tension of the surrounding liquid comes into play. In general, different nonlinear effects can be observed depending on the equilibrium radius of the coated bubble, which is usually included in $]R_b, R_r[$.

To sum up, we can hypothesize that

$$p_{uca} = p_G(R,t) - p_0 - p_a(t) - \frac{2\sigma_S(R)}{R} - \frac{4(\mu_L)\dot{R}}{R} - p_{vis}. \tag{111}$$

In the linear regime of small-amplitude oscillations, the presence of new terms with respect to p_L of (1) will lead to differences in the damping coefficients β and in the natural frequencies ω_0 introduced in (6) and (7).

In order to determine the polytropic index through the linearization of the gas dynamics equations, the calculations proposed for monatomic gases in Sec. V and generalized to polyatomic gases in VI are identical: the only difference will be found in the value of w, which in the presence of the shell will be $w = 2\sigma_S(R_0)/(p_0 R_0)$ with $\sigma_S(R_0) \in]0, \sigma_L[$. Figure 24 presents the possible effects on κ in the presence of a shell. To achieve this, we prescribed $R_0 = 10^{-6}$ m and values of the other physical constants at standard environmental conditions, and we referred to carbon dioxide gas for two different values of the bulk viscosity (CO_2 gas has actually been employed for the production of some types of UCAs[74,75]). Furthermore, we ignored mass transfer and we set the temperature at bubble boundary to be the same as the liquid, even if a thicker shell could have thermal insulation effects that should be taken into account. As often proposed in the literature, we assumed the coated bubble to be immersed in water: naturally, this hypothesis is made for simple experiments, while in real applications UCAs are located in blood vessels or in soft tissues.

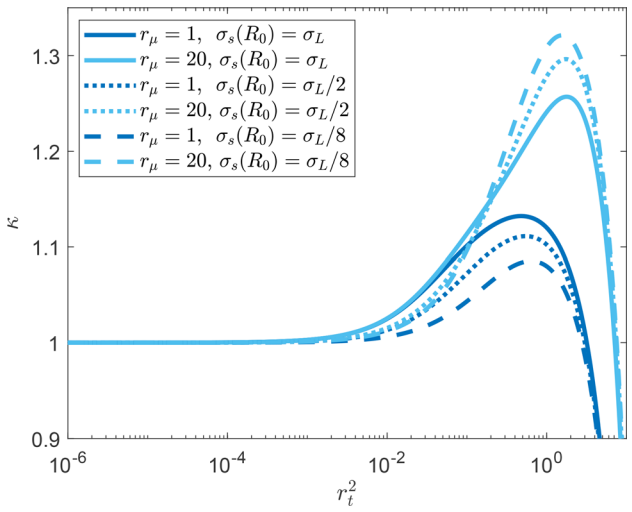

FIG. 24. A comparison between polytropic indexes calculated for different values of $\sigma_s(R_0)$ and bulk viscosity, for a coated bubble filled with CO_2 with equilibrium radius $R_0 = 10^{-6}$ m. The gas dynamics is described by the RET model, and in *case a*, boundary conditions are imposed.

XII. THE ROLE OF SURFACTANTS AND VISCOELASTIC MATERIALS

Recently, the role of surfactants in the liquid containing the bubble has been extensively studied both theoretically and experimentally due to their stabilizing effects. Again, these are mostly nonlinear phenomena that are beyond the scope of this discussion. We limit ourselves to observing that in the linear regime, it is possible to account for a reduction in surface tension, the consequences of which are similar to those already reported for shells.[76–78]

Regarding the study of gas bubbles immersed in a viscoelastic material (especially soft tissues, given their numerous biomedical applications),[79] a wide variety of models is available in the literature for viscoelastic solids or liquids. In these cases, one often starts with a modification of the Rayleigh–Plesset equation (1) or the Keller–Miksis one (2) to account for the contribution due to the deviatoric part of the stress tensor and the strain of the medium. The constitutive equations that relate these physical quantities to bubble radius and its time derivative vary depending on the assumption introduced.

If we limit ourselves to examining linear viscoelastic models, we can cite studies that include viscous and elastic effects of Kelvin–Voigt materials.[79,80] In this framework, the equation of the damped and forced linear oscillator (6) obtained from the Taylor series expansion of the ODE for the bubble radius is modified. In particular, additional terms proportional to the shear modulus appear in both the natural pulsation and the damping coefficient. However, the gas pressure and its equilibrium value, p_G and p_{GE}, are unchanged, and therefore the calculation of κ and μ_G remains the same as those already illustrated in Secs. V and VI.

Linear models such as Maxwell's give rise to more complex equations[81] for which it is usually not reasonable to exclude nonlinear effects.

XIII. CONCLUSIONS

This work is the first systematic study of the role played by RET models in bubble dynamics. It was possible to verify that for large bubbles or monatomic gases, RET and NSF are in perfect agreement, while this is no longer true when spatial scales are smaller and the bulk viscosity of the gas is taken into account. RET thus proves to be a model capable of describing phenomena associated with bubbles of different sizes (also in the cases involving small amplitude oscillations), including those traditionally well represented by NSF.

Here, we analyzed different parameters and physical conditions by relating them to the linear behavior of a gas bubble under the action of a forcing acoustic pressure. The analytic small-amplitude solutions were always explicitly determined. However, to make comparisons simpler and more immediate, we plotted only two quantities related to the behavior of gas pressure and bubble wall: polytropic index κ and damping coefficient β_G.

Still taking thermal effects into account, the impact of gas parameters (such as molecular mass, shear, and bulk viscosity) was explored, also finding or verifying results already known in the literature. In particular, the deviatoric part of the stress tensor appears to be negligible

10 January 2026 08:22:20

© Author(s) 2025

even for the RET equations in various geometric symmetries, with the exception of situations of little physical interest.

Different thermal conditions were introduced at the gas–liquid interface, the mass transfer condition was examined, and the consequences of the presence of a shell were studied as well. As expected, the size and shape of the bubble could have a significant impact on small-amplitude oscillations: in particular, to our knowledge, the effects of geometry on κ were analyzed and compared for the first time. Furthermore, homobaric RET models were built for various geometries, and the range of validity of the homobaric hypothesis was investigated. The importance of these results lies in the fact that such models are commonly used in the literature in the case of nonlinear oscillations in order to simplify numerical integration. In addition, the combined effect of two or more physical parameter variations can be appreciated by comparing the above figures.

This preliminary analysis has several purposes. First, it provides the starting point for the rational use of gas models (in particular RET ones) even in conditions far from the regime of small-amplitude oscillations, when numerical techniques and further simplifications are required to obtain solutions. We are already working on this point in different frameworks that also include multi-bubble systems.

Moreover, the present outcomes are about to be applied to bubbly liquids under small acoustic forcing conditions.

Another long-standing issue concerns the modeling of gas dynamics starting from a simple polytropic process. This is a highly simplified approach used to make the integration of the bubble radius/volume equation quick and easy, while neglecting thermal effects. We hope that what we have obtained here will offer food for thought regarding the choice of κ, particularly when dealing with micro- or nano-bubbles.

Unfortunately, to the best of our knowledge, there are currently no experimental data available that allow for quantitative comparisons and validations, but hopefully there will be new measurements in the near future.

Finally, special attention will be paid to recent research trends in the field of UCAs and viscoelastic media (see, for example, Refs. 73 and 82–85). The linear analysis conducted in the previous sections (XI–XII) clearly suggests that for small bubbles ($R_0 \in [10^{-6}, 10^{-9}]$ m) containing polyatomic gases, RET theory could offer significant contributions in the interpretation of experimental data and in the prediction of phenomena, even in the nonlinear regime.

ACKNOWLEDGMENTS

The authors would like to thank the anonymous reviewers for their helpful comments and suggestions. The paper was supported by Gruppo Nazionale di Fisica Matematica (GNFM) dell'INdAM and in part (F.B.), by the Italian research Project PRIN 2022 CUP: D53D23003020006 "The Mathematics and Mechanics of Nonlinear Wave Propagation in Solids."

AUTHOR DECLARATIONS

Conflict of Interest

The authors have no conflicts to disclose.

Author Contributions

F. Brini: Conceptualization (equal); Formal analysis (equal); Investigation (equal); Methodology (equal); Software (equal); Validation (equal); Writing – original draft (equal). **L. Seccia:** Conceptualization (equal); Methodology (equal); Writing – original draft (equal).

DATA AVAILABILITY

The data that support the findings of this study are available within the article.

APPENDIX: THE BESSEL FUNCTIONS OF FIRST KIND

For $n \in \mathbb{N}$, the Bessel functions of the first and second kind, denoted, respectively, by $J_n(s)$, $Y_n(s)$, are solutions of the ODE (where f is a generic function)

$$s^2 \frac{d^2 f(s)}{ds^2} + s \frac{df(s)}{ds} + (s^2 - n) f(s) = 0.$$

They can be expressed as

$$J_n(s) = \sum_{j=0}^{\infty} \frac{(-1)^j}{j!\Gamma(n+j+1)} \left(\frac{s}{2}\right)^{2j+n},$$

$$Y_n(s) = \frac{J_n(s)\cos(n\pi) - J_{-n}(s)}{\sin(n\pi)}.$$

Since the limit of Y_n for $s \to 0$ diverges, while $J_n(s)$ converges to a finite value [and in particular, $J_{2n}(0) = 0$], the presence of second-kind functions is excluded from the construction of the solutions in Secs. VII–IX. For this reason, we report here only the main properties of $J_n(s)$ that were used in the previous pages

$$\frac{d(s^n J_n(s))}{ds} = s^n J_{n-1}(s), \quad \frac{dJ_n(s)}{ds} = \frac{n}{s} J_n(s) - J_{n+1}(s),$$
$$J_{-n}(s) = (-1)^n J_n(s), \quad J_n(-s) = (-1)^n J_n(s),$$
$$sJ_{n+1}(s) = 2nJ_n(s) - sJ_{n-1}(s).$$

In particular, with regard to the last formula, it turns out that for any value of $n \in \mathbb{N}$ $J_n(s)$ can be expressed as combinations of $J_0(s)$ and $J_1(s)$.

REFERENCES

[1]Lord Rayleigh, "On the pressure developed in a liquid during the collapse of a spherical cavity," Philos. Mag. **34**, 94 (1917).
[2]M. S. Plesset, "The dynamics of cavitation bubbles," J. Appl. Mech. **16**, 277 (1949).
[3]W. Lauterborn, "Numerical investigation of nonlinear oscillations of gas bubbles in liquids," J. Acoust. Soc. Am. **59**, 283 (1976).
[4]M. S. Plesset and A. Prosperetti, "Bubble dynamics and cavitation," Annu. Rev. Fluid Mech. **9**, 145 (1977).
[5]A. Prosperetti, L. A. Crum, and K. Commander, "Nonlinear bubble dynamics," J. Acoust. Soc. Am. **83**, 502 (1988).
[6]R. Loefstedt, B. P. Barber, and S. J. Putterman, "Toward a hydrodynamic theory of sonoluminescence," Phys. Fluids A **5**, 2911 (1993).
[7]T. G. Leighton, *The Acoustic Bubble* (Academic Press, 1994).
[8]B. P. Barber, R. A. Hiller, S. J. Putterman, and K. R. Weninger, "Defining the unknowns of sonoluminescence," Phys. Rep. **281**, 65 (1997).
[9]A. Prosperetti and Y. Hao, "Modelling of spherical gas bubble oscillations and sonoluminescence," Philos. Trans. R. Soc., Ser. A **357**, 203 (1999).
[10]S. J. Putterman and K. R. Weninger, "Sonoluminescence: How bubbles turns sound into light," Annu. Rev. Fluid Mech. **32**, 445 (2000).

10 January 2026 08:22:20

© Author(s) 2025

[11]M. P. Brenner, S. Hilgenfeldt, and D. Lohse, "Single-bubble sonoluminescence," Rev. Mod. Phys. **74**, 425 (2002).
[12]H. Lin, B. Storey, and A. J. Szeri, "Inertially driven inhomogeneities in violently collapsing bubbles: The validity of the Rayleigh-Plesset equation," J. Fluid Mech. **452**, 145 (2002).
[13]A. Prosperetti, "Bubbles," Phys. Fluids **16**, 1852 (2004).
[14]W. Lauterborn and T. Kurz, "Physics of bubble oscillations," Rep. Prog. Phys. **73**, 106501 (2010).
[15]G. Zhou and A. Prosperetti, "Modelling the thermal behaviour of gas bubbles," J. Fluid Mech. **901**, R3 (2020).
[16]A. M. Zhang, S. M. Li, R. Z. Xu, S. C. Pei, S. Li, and Y. L. Liu, "A theoretical model for compressible bubble dynamics considering phase transition and migration," J. Fluid Mech. **999**, A58 (2024).
[17]C. E. Brennen, "Cavitation in medicine," Interface Focus **5**, 20150022 (2015).
[18]Y. Guo, H. Lee, C. Kim, C. Park, A. Yamamichi, P. Chuntova, M. Gallus, M. O. Bernabeu, H. Okada, H. Jo, and C. Avanitis, "Ultrasound frequency-controlled microbubble dynamics in brain vessels regulate the enrichment of inflammatory pathways in the blood-brain barrier," Nat. Commun. **15**, 8021 (2024).
[19]D. A. Fernandes, "Comprehensive review on bubbles: Synthesis, modification, characterization and biomedical applications," Bioconjugate Chem. **35**, 1639 (2024).
[20]Z. Pandur, J. Zevnik, D. Podbevesek, B. Stojkovic, and D. Stopar, "Water treatment by cavitation: Understanding it at a single bubble-bacterial cell level," Water Res. **236**, 119956 (2023).
[21]F. Grieser, P. Choi, N. Enomoto, H. Harada, K. Okitsu, and K. Yasui, *Sonochemistry and the Acoustic Bubble* (Elsevier, 2015).
[22]C. Wang, R. Tao, J. Wu, H. Jiang, Z. Hu, B. Wang, and Y. Yang, "Sonochemistry: Materials science and engineering applications," Coord. Chem. Rev. **526**, 216373 (2025).
[23]K. W. Commander and A. Prosperetti, "Linear pressure waves in bubbly liquids: Comparison between theory and experiments," J. Acoust. Soc. Am **85**, 732 (1989).
[24]A. Prosperetti, "The speed of sound in a gas-vapor bubbly liquid," Interface Focus **5**, 20150024 (2015).
[25]J. Liang and J. Liu, "Dynamics of three cavitation bubbles with pulsation and symmetric deformation," Ultrason. Sonochem. **96**, 106428 (2023).
[26]K. D. Hattori and T. Yamamotoi, "Mass transfer of acoustic cavitation bubbles in multi-bubble environment," Ultrason. Sonochem. **115**, 107295 (2025).
[27]R. Z. Xie, S. M. Li, J. H. Xing, P. P. Wang, and A. M. Zhang, "Theoretical analysis of the dynamic characteristics of a spatial three-bubble system," Phys. Fluids **37**, 093303 (2025).
[28]I. Mueller and T. Ruggeri, *Rational Extended Thermodynamics* (Springer, New York, 1998).
[29]T. Ruggeri and M. Sugiyama, *Classical and Relativistic Rational Extended Thermodynamics of Gases* (Springer, New York, 2021).
[30]F. Brini and L. Seccia, "Acceleration waves and oscillating gas bubbles modelled by rational extended thermodynamics," Proc. R. Soc. A **478**, 2022.0246 (2022).
[31]F. Brini and L. Seccia, "Acceleration waves in cylindrical shrinking gas bubbles," Nucl. Sci. Eng. **197**, 2301 (2023).
[32]F. Brini and L. Seccia, "The role of the dynamic pressure in the behavior of an oscillating gas bubble," Phys. Fluids **36**, 097151 (2024).
[33]A. Prosperetti, "Thermal effects and damping mechanisms in the forced radial oscillations of gas bubbles in liquid," J. Acoust. Soc. Am. **61**, 17 (1977).
[34]F. R. Gilmore, "The growth or collapse of a spherical bubble in a viscous compressible liquid," Technical Report No. 26-4 (Hydrodynamics Laboratory, California Institute of Technology, Pasadena, CA, 1952).
[35]J. B. Keller and M. Miksis, "Bubble oscillations of large amplitude," J. Acoust. Soc. Am. **68**, 628 (1980).
[36]A. M. Zhang, S. M. Li, P. Cui, and S. Li, "A unified theory for bubble dynamics," Phys. Fluids **35**, 033323 (2023).
[37]A. Prosperetti, "The thermal behaviour of oscillating gas bubbles," J. Fluid Mech. **222**, 587 (1991).
[38]A. Prosperetti, "Nonlinear oscillations of gas bubbles in liquids: Steady-state solutions," J. Acoust. Soc. Am. **56**, 878 (1974).
[39]M. Minnaert, "On musical air-bubbles and the sounds of running water," London, Edinburgh Dublin Philos. Mag. J. Sci. **16**, 235 (1933).
[40]E. Ikenberry and C. Truesdell, "On the pressures and the flux of energy in a gas according to Mawell's kinetic theory, I," Indiana Univ. Math. J. **5**, 1 (1956).
[41]T. Arima, S. Taniguchi, T. Ruggeri, and M. Sugiyama, "Extended thermodynamics of dense gases," Continuum Mech. Thermodyn. **24**, 271 (2012).
[42]T. Arima, M. Carrisi, S. Pennisi, and T. Ruggeri, "Which moments are appropriate to describe gases with internal structure in rational extended thermodynamics?," Int. J. Non-Linear Mech. **137**, 103820 (2021).
[43]J. F. Bourgat, L. Desvillettes, P. L. Tallec, and B. Perthame, "Microreversible collisions for polyatomic gases and Boltzmann's theorem," Eur. J. Mech. B-fluids **13**, 237 (1994).
[44]F. Brini and T. Ruggeri, "Hyperbolicity of first and second order extended thermodynamics theory of polyatomic rarefied gases," Int. J. Non-Linear Mech. **124**, 103517 (2020).
[45]C. Truesdell, "The physical components of vector and tensor," ZAMM **33**, 345 (1953).
[46]M. S. Cramer, "Numerical estimates for the bulk viscosity of ideal gases," Phys. Fluids **24**, 066102 (2012).
[47]F. Jaeger, O. K. Matar, and E. A. Mueller, "Bulk viscosity of molecular fluids," J. Chem. Phys. **148**, 174504 (2018).
[48]A. S. Meijer, A. S. de Wijn, M. F. E. Peters, N. J. Dam, and W. van de Water, "Coherent Rayleigh–Brillouin scattering measurements of bulk viscosity of polar and nonpolar gases, and kinetic theory," J. Chem. Phys. **133**, 164315 (2010).
[49]Y. Wang, W. Ubachs, and W. van de Water, "Bulk viscosity of CO_2 from Rayleigh-Brillouin light scattering spectroscopy at 532 nm," J. Chem. Phys. **150**, 154502 (2019).
[50]B. Sharma and R. Kumar, "Estimation of bulk viscosity of dilute gases using a nonequilibrium molecular dynamics approach," Phys. Rev. E **100**, 013309 (2019).
[51]E. Kustova, M. Mekhonoshina, and A. Kosareva, "Relaxation processes in carbon dioxide," Phys. Fluids **31**, 046104 (2019).
[52]S. Kosuge and K. Aoki, "Shock-wave structure for a polyatomic gas with large bulk viscosity," Phys. Rev. Fluids **3**, 023401 (2018).
[53]S. Taniguchi, T. Arima, T. Ruggeri, and M. Sugiyama, "Effect of dynamic pressure on the shock structure in a rarefied polyatomic gas," Phys. Fluids **26**, 016103 (2014).
[54]T. Arima, E. Barbera, F. Brini, and M. Sugiyama, "The role of the dynamic pressure in stationary heat conduction of a rarefied polyatomic gas," Phys. Lett. A **378**, 2695 (2014).
[55]E. Barbera, F. Brini, and M. Sugiyama, "Heat transfer problem in a van der Waals gas," Acta Appl. Math. **132**, 41 (2014).
[56]T. Arima and M. Sugiyama, "A novel effect of dynamic pressure on a nonequilibrium flow of a rarefied polyatomic gas through a diverging nozzle," Phys. Lett. A **476**, 128881 (2023).
[57]T. Ruggeri and S. Taniguchi, "Effect of dynamic pressure on the shock structure and sub-shock formation of a mixture of polyatomic gases," Commun. Appl. Math. Comput. **6**, 2196 (2024).
[58]J. R. Rumble, *CRC Handbook of Chemistry and Physics* (CRC Press, Boca Raton, FL, 2022).
[59]A. Marmur, C. D. Volpe, S. Siboni, A. Amirfazli, and J. W. Drelich, "Contact angles and wettability: Towards common and accurate terminology," Surf. Innovations **5**, 3 (2017).
[60]J. Feng, J. Yuan, and S. K. Cho, "Micropropulsion by an acoustic bubble for navigating microfluidic spaces," Lab Chip **15**, 1554 (2015).
[61]Y. A. Ilinskii, E. A. Zabolotskaya, T. A. Hay, and M. F. Hamilton, "Models of cylindrical bubble pulsation," J. Acoust. Soc. Am. **132**, 1346 (2012).
[62]A. A. Doinikov, T. Combriat, P. Thibault, and P. Marmottant, "Acoustic streaming produced by a cylindrical bubble undergoing volume and translational oscillations in a microfluidic channel," Phys. Rev. E **94**, 033109 (2016).
[63]J. Yu, J. Luo, X. Zhang, Y. Zhang, and Y. Zhang, "Multi-scale analysis of harmonic resonance in cylindrical bubbles under acoustic excitation," Phys. Fluids **36**, 093310 (2024).
[64]B. Dollet, S. M. Van Der Meer, V. Garbin, N. De Jong, D. Lohse, and M. Versluis, "Nonspherical oscillations of ultrasound contrast agents microbubbles," Ultrasound Med. Biol. **34**, 1465 (2008).
[65]A. Prosperetti, "Vapor bubbles," Annu. Rev. Fluid Mech. **49**, 221 (2017).
[66]L. Bergamasco and D. Fuster, "Oscillation regimes of gas/vapor bubbles," Int. J. Heat Mass Transfer **112**, 72 (2017).

10 January 2026 08:22:20

© Author(s) 2025

[67]S. Fujikawa and T. Akamatsu, "Effects of the non-equilibrium condensation of vapour on the pressure wave produced by the collapse of a bubble in a liquid," J. Fluid Mech. **97**, 481 (1980).
[68]P. S. Epstein and M. S. Plesset, "On the stability of gas bubbles in liquid-gas solutions," J. Chem. Phys. **18**, 1505 (1950).
[69]A. Eller and H. G. Flynn, "Rectified diffusion during nonlinear pulsations of cavitation bubbles," J. Acoust. Soc. Am. **37**, 493 (1965).
[70]C. C. Church, "The effect of an elastic solid surface layer on the radial pulsation of gas bubbles," J. Acoust. Soc. Am. **97**, 1510 (1995).
[71]N. de Jong, R. Cornet, and C. T. Lancée, "Higher harmonics of vibrating gas-filled microspheres. Part one: Simulations," Ultrasonics **32**, 447 (1994).
[72]P. Marmottant, S. van der Meer, M. E. M. Versluis, N. de Jong, S. Hilgenfeldt, and D. Lohse, "A model for large amplitude oscillations of coated bubbles accounting for buckling and rupture," J. Acoust. Soc. Am. **118**, 3499 (2005).
[73]T. Kanagawa, M. Honda, and Y. Kikuchi, "Nonlinear acoustic theory on flowing liquid containing multiple microbubbles coated by a compressible viscoelastic shell: Low and high frequency cases," Phys. Fluids **35**, 023303 (2023).
[74]F. Ali, M. A. Mangi, H. Rehman, and E. Kaluski, "Use of carbon dioxide as an intravascular contrast agent: A review of current literature," World J. Cardiol. **9**, 715 (2017).
[75]S. Quaglino, E. Ferrero, M. Ferri, P. Manzo, M. Lanza, A. Ricotti, and A. Gaggiano, "Safety, effectiveness and pitfalls of carbon dioxide routine use as a contrast agent for endovascular abdominal aortic repair," Ann. Vasc. Surg. **101**, 120 (2024).
[76]S. Takagi and Y. Matsumoto, "Surfactant effects on bubble motion and bubbly flows," Annu. Rev. Fluid Mech. **43**, 615 (2011).
[77]M. Pang, M. Jia, and Y. Fei, "Experimental study on effect of surfactant and solution property on bubble rising motion," J. Mol. Liquids **375**, 121390 (2023).
[78]L. Vobecka, S. Orvalho, M. Zednikova, J. Veejrazka, and J. Tihon, "Damping effect of surfactants on induced bubble shape deformations," Phys. Fluids **35**, 122120 (2023).
[79]B. Dollet, P. Marmottant, and V. Garbin, "Bubble dynamics in soft and biological matter," Annu. Rev. Fluid Mech. **51**, 331 (2019).
[80]X. Yang and C. C. Church, "A model for the dynamics of gas bubbles in soft tissue," J. Acoust. Soc. Am. **118**, 3595 (2005).
[81]J. S. Allen and R. A. Roy, "Dynamics of gas bubbles in viscoelastic fluids. I. Linear viscoelasticity," J. Acoust. Soc. Am. **107**, 3167 (2000).
[82]M. Versluis, E. Stride, G. Lajoinie, B. Dollet, and T. Segers, "Ultrasound contrast agent modeling: A review," Ultrasound Med. Biol. **46**, 2117 (2020).
[83]K. Murakami, Y. Yamakawa, J. Y. Zhao, E. Johnsen, and K. Ando, "Ultrasound-induced nonlinear oscillations of a spherical bubble in a gelatin gel," J. Fluid Mech. **924**, A 38 (2021).
[84]A. K. Abu-Nab, A. M. Morad, E. S. Selima, T. Kanagawa, and A. F. Abu-Bakr, "A review of microcavitation bubbles dynamics in biological systems and their mechanical applications," Ultrason. Sonochem. **121**, 107521 (2025).
[85]X. Shen, P. Wu, and W. Lin, "Numerical simulation of cavitation threshold in water and viscoelastic medium based on bubble cluster dynamics," Ultrason. Sonochem. **119**, 107414 (2025).

10 January 2026 08:22:20

© Author(s) 2025